



Mean field fracture in disordered solids: Statistics of fluctuations

Hudson Borja da Rocha^{a,*}, Lev Truskinovsky^b

^a CIRB, CNRS UMR 7241, INSERM U1050, Collège de France and PSL Research University, F-75005 Paris, France

^b PMMH, CNRS-UMR 7636 PSL-ESPCI, 10 Rue Vauquelin, 75005 Paris, France

ARTICLE INFO

Keywords:

Fracture
Criticality
Brittle to ductile
Fluctuations

ABSTRACT

Power law distributed fluctuations are known to accompany *terminal* failure in disordered brittle solids. The associated intermittent scale-free behavior is of interest from the fundamental point of view as it emerges universally from an intricate interplay of threshold-type nonlinearity, quenched disorder, and long-range interactions. We use the simplest mean-field description of such systems to show that they can be expected to undergo a transition between brittle and quasi-brittle (ductile) responses. While the former is characterized by a power law distribution of avalanches, in the latter, the statistics of avalanches is predominantly Gaussian. The realization of a particular regime depends on the variance of disorder and the effective rigidity represented by a combination of elastic moduli. We argue that the robust criticality, as in the cases of earthquakes and collapsing porous materials, indicates the self-tuning of the system towards the boundary separating brittle and ductile regimes.

1. Introduction

While many engineering aspects of fracture in intrinsically disordered solids have been thoroughly investigated (Krajcinovic and Van Mier, 2000; Bazant and Le, 2017; Curtin, 1998), the statistical properties of fracture-induced fluctuations have become a subject of focused research only recently (Herrmann and Roux, 2014; Alava et al., 2006; Fortin et al., 2009; Petri et al., 1994; Tordesillas et al., 2020). The interest towards fluctuations is mostly driven by experimental observations revealing that acoustic emission measured prior to *terminal* fracture and the roughness of the ensuing fracture surface are described by scale-free laws, indicating turbulence-type complexity and suggesting criticality (Bonamy and Bouchaud, 2011; Bouchbinder et al., 2014; Girard et al., 2010; Baró et al., 2018; Vu et al., 2019). Power law distributed spatial and temporal fluctuations in disordered brittle solids are also of interest from the fundamental point of view because of the intricate interplay in the underlying processes between threshold-type, strong nonlinearity, quenched disorder and long-range interactions (Biswas et al., 2015; Sahimi, 1998). Of practical importance is the accurate prediction of the terminal failure through the identification of the precursors for the catastrophic coalescence of micro-fractures (Bažant, 2019; Ray, 2019; Sornette, 2002).

The observed scale-free behaviors in fracturing solids have been linked, by some authors, to thermodynamic spinodal points associated with first-order phase transitions (Alava et al., 2006; Zapperi et al., 1997) and, by other authors, to critical points or second-order phase transitions (Moreno et al., 2000; Weiss et al., 2014; Vu et al., 2019; Garcimartín et al., 1997). An additional complication here is that athermal fracture can be modeled in two different ways: as an incremental *global* energy minimization (GM) phenomenon (zero-temperature limit of a thermal equilibrium response), e.g. (Francfort and Marigo, 1998; Bourdin et al., 2008) or as an incremental *local* energy minimization keeping the system in the state of marginal stability (MS) (zero viscosity limit of an overdamped response), e.g. (Selinger et al., 1991; Wang et al., 1991; Puglisi and Truskinovsky, 2005).

* Corresponding author.

E-mail addresses: hudson.borja-da-rocha@polytechnique.edu (H. Borja da Rocha), lev.truskinovsky@espci.fr (L. Truskinovsky).

The statistical physics approach to fracture is usually based on direct simulation of discrete models, which carry a regularizing internal length scale, allow for a relatively simple introduction of disorder (Hansen and Roux, 2000) and are suitable for the inclusion of thermal noise (Politi et al., 2002; Roux, 2000; Borja da Rocha and Truskinovsky, 2019). In such models, the continuum medium is represented by a network of elastic elements while the disorder is modeled either by random failure thresholds or by random elimination of the elements. Crucially, the discrete models retain the long-range nature and the tensorial structure of the elastic interactions (Nikolić et al., 2018; Ostoja-Starzewski, 2007).

Many important discoveries in statistical fracture mechanics were made based on the study of the discrete random fuse model (RFM) in which a scalar field represents displacements, elasticity is linear, but the threshold nature of fracture is preserved (de Arcangelis et al., 1985). And still, RFM is too complex to be amenable to analytical study, so further simplifications were made to allow for theoretical analysis. The desired analytical transparency was achieved (without losing the main effects) in the framework of the exactly solvable global load sharing (GLS) fiber bundle model (FBM) (Hansen et al., 2015), which can be seen as a mean-field approximation of the RFM. More comprehensive continuum modeling approaches, including phase field (Berthier et al., 2017, 2021; Gorgogianni et al., 2020) and mesoscopic damage models (Girard et al., 2010; Patinet et al., 2014) are still mostly numerical.

In this paper, we use the augmented GLS model to show that both spinodal and critical *scaling behaviors* are relevant near the threshold of the brittle-to-ductile transition, which is characteristic for such systems (Liu et al., 2019; Selezneva et al., 2018). The ductile response is understood here in the sense of stable development of small avalanches representing micro-failure events (Christensen et al., 2018), while the brittle response is defined by an abrupt macro-failure event representing system-size instability (Papanikolaou et al., 2019; Berthier et al., 2019). This abruptness is the consequence of stress concentration in the system that induces an autocatalytic bond-breaking process. In ductile systems such catastrophic breaking is absent, and as a consequence, the mechanical response in the ductile regime is gradual, persisting after the stress peak. The signature of ductile fracture is that the fracture toughness is large, the inelastic deformation is spatially diffuse, and the failure is gradual. Instead, the fracture toughness associated with a brittle fracture is small, and the inelastic deformation is localized. Understanding the microscopic spatio-temporal processes behind the stochastization near the brittle-to-ductile (BDT) transition and revealing the statistical structure of the associated intermittent fluctuations is one of the most important challenges in statistical fracture mechanics.

To study these intriguing phenomena *analytically* we needed to go beyond the simplest GLS model, even though it has proved successful in describing a variety of physical phenomena from the failure of textiles and acoustic emission in loaded composites to earthquake dynamics (Nechad et al., 2005; Xia et al., 2001; Pradhan et al., 2010). The problem is that in all these applications, the fracture development could be studied in a stress control (soft device) setting, where the ultimate failure is necessarily *brittle*. As a result, the terminal fracture is accompanied by standard fluctuations exhibiting universal scaling of spinodal type (Hemmer and Hansen, 1992; Hansen et al., 2015; Sornette, 1989; Kloster and Hemmer, 1997). Various “non-democratic” settings of FBM, implying local load sharing, have also been studied in the soft device setting, which ultimately obscures the BDT transition (Pradhan et al., 2010; Patinet et al., 2014; Delaplace et al., 1999).

To capture the ductile behavior and to be able to *tune* the system to criticality, we had to address failure under strain control (hard device) (Delaplace et al., 1999). To this end, in this paper, we introduced two seemingly innocent extensions of the standard FBM in the form of additional internal (series to fibers) and external (series to the bundle) linear springs. The main advantage of the new framework is that by changing the relative stiffness of the internal and external springs, one can simulate the crossover from brittle to ductile response. Interestingly, we found that the augmented FBM exhibits different types of scaling in these two regimes: brittle failure emerges as a supercritical, while ductile failure comes out as a subcritical phenomenon. The *critical* behavior can be associated with the BDT transition only, and we show that due to the superuniversality of mean-field models (Balog et al., 2014), the MS and GM critical exponents are the same.

The augmented FBM also reveals the parallel roles of disorder and the effective rigidity (represented here by the strategic ratio of elastic moduli) as the two main *regulators* of the BDT transition (Merkel et al., 2019; Driscoll et al., 2016; Zhang et al., 2017; Dussi et al., 2020; Borja da Rocha and Truskinovsky, 2020; Richard et al., 2021; David et al., 2021) separating ductile behavior at low rigidity and high disorder from the brittle behavior at low disorder and high rigidity. Since both ductility and brittleness represent the material response outside the elastic limit, the emergence of an elastic control through the effective rigidity may appear counter-intuitive in this context. We recall, however, that the inelastic mechanical response is intimately related to the microscopic structure of the crystal. For instance, the manner in which stress is redistributed in response to intrinsic instabilities (representing inelastic effects) depends on both the strength and the topology of atomic bonding. In particular, the parameters of the BDT transition are known to be highly sensitive to the internal connectivity of the crystal lattice represented either by the Poisson’s ratio or by the ratio of bulk to shear modulus (Greaves et al., 2011). In this paper, we show that in addition to influencing the failure mode, such ratios can also fundamentally affect the fluctuational precursors of the macro-instability, which can be then used to build statistical predictors of the ultimate structural failure.

The rest of the paper is organized as follows. In Section 2, we introduce the model and analyze the averaged response. The empirical avalanche distributions, emerging from direct numerical simulation of the model, are studied in Section 3. Then in Section 4, we build a mapping between the micro-fracture avalanches and biased random walks which allows us to compute analytically their statistical characteristics in both MS and GM regimes. The asymptotic scaling laws for brittle, critical, and ductile behaviors are derived in Section 5. The finite-size scaling is studied in Section 6. Finally, in Section 7, we present our conclusions.

Some of the results of this paper were first announced in (Borja da Rocha and Truskinovsky, 2020).

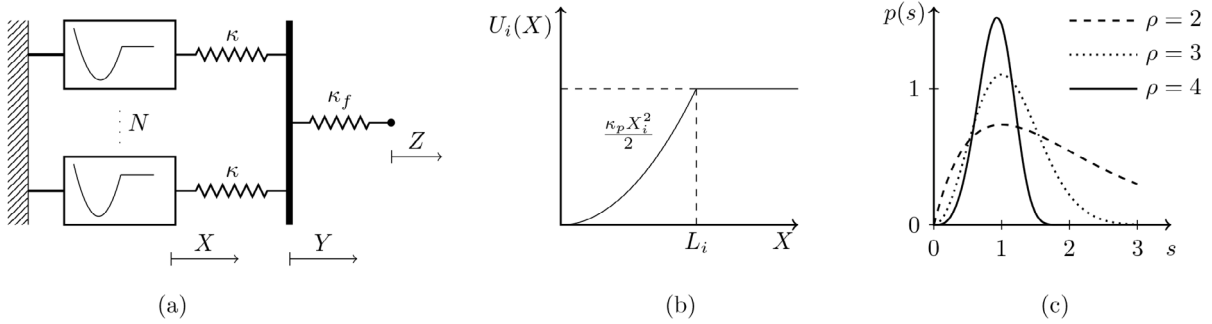


Fig. 1. (a) Mechanical model of the system, (b) the potential energy of a single bond and (c) Weibull distribution of the debonding thresholds $p(s)$ at different values of the parameter ρ .

2. The model

Consider N parallel breakable elastic links and suppose that a link with index $i = 1, \dots, N$ is characterized by a breaking threshold L_i . Assume further that the system is loaded through a load redistributing medium modeled as an external spring with stiffness κ_f (Delaplace et al., 1999). The total energy of the system can be written as,

$$E = \sum_i^N U_i(X_i) + \frac{\kappa}{2} \sum_i^N (Y - X_i)^2 + \frac{\kappa_f}{2} (Z - Y)^2, \tag{1}$$

where Y is a position of the connecting backbone and Z is the total elongation serving as the controlling parameter, see Fig. 1(a). The nonlinear breakable element is characterized by the potential, $U_i(X) = \kappa_p X^2/2$ for $X \leq L_i$ and $U_i(X) = \kappa_p L_i^2/2$ for $X > L_i$. The variable X_i represents the internal degree of freedom of the unit i . For values of X_i smaller than L_i the element is attached to the backbone and bears the same force as the other bound units. When the variable X_i reaches the threshold L_i the i 'th element breaks, dissipating (or transforming into a non mechanical form) the energy $\kappa_p L_i^2/2$.

It will be convenient to work with dimensionless variables. We define the reference scale ℓ_0 to be the resting length of the linear springs, and introduce the dimensionless variables $x_i = X_i/\ell_0$, $y = Y/\ell_0$, $z = Z/\ell_0$ and $l_i = L_i/\ell_0$. The remaining non-dimensional parameters of the problem are $\lambda = \kappa/\kappa_p$ and $\lambda_f = \kappa_f/(N\kappa_p)$. The dimensionless energy per element in a hard device is given by

$$\mathcal{H}(\mathbf{x}, y, z) = \frac{1}{N} \sum_{i=1}^N \left[u_i(x_i) + \frac{\lambda}{2} (y - x_i)^2 \right] + \frac{\lambda_f}{2} (z - y)^2. \tag{2}$$

where, $u_i(x) = x^2/2$ for $x \leq l_i$ and $u_i(x) = l_i^2/2$ for $x > l_i$. We assume that the failure thresholds l_i are *disordered* and represented by independent random variables each described by the same probability density $p(s)$, and the same cumulative distribution $P(s) = \int_0^s p(y)dy$. The soft device loading can be seen as a limiting case of the hard device loading; it can be obtained if we assume that the outer spring is infinitely soft $\lambda_f \rightarrow 0$. In this limit $z \rightarrow \infty$, but if simultaneously $\lambda_f z \rightarrow f$ we obtain the system loaded by the force f .

To explore the set of the metastable states we need to first equilibrate the system with respect to the internal variables x_i 's and y . To this end, we need to solve the system of equations:

$$\begin{cases} \frac{\partial \mathcal{H}}{\partial x_i} = 0, \text{ for all } 1 \leq i \leq N \\ \frac{\partial \mathcal{H}}{\partial y} = 0. \end{cases} \tag{3}$$

Equilibration in \mathbf{x} gives $u'(x_i) = \lambda(y - x_i)$, or more explicitly, $x_i = x_0$ for $x_i \leq l_i$ and $x_i = x_{00}$ for $x_i > l_i$, where $x_0 = \lambda y/(\lambda + 1)$ and $x_{00} = y$. The equilibration in y gives,

$$y(\mathbf{x}, z) = \frac{1}{\lambda + \lambda_f} \left(\lambda_f z + \lambda \frac{1}{N} \sum_{i=1}^N x_i \right). \tag{4}$$

We see the mean-field nature of the coupling through Eq. (4): the variable y is affected by the average value of x_i . Using permutational invariance we can write

$$\frac{1}{N} \sum_{i=1}^N x_i = \frac{k}{N} y + \frac{N - k}{N} \frac{\lambda y}{\lambda + 1} \tag{5}$$

where k is the number of broken bonds. This representation allows us to write the equilibrium elongation \hat{y} as a function of the total elongation z :

$$\hat{y}(k, z) = \frac{\Lambda z}{1 - k/N + \Lambda}. \tag{6}$$

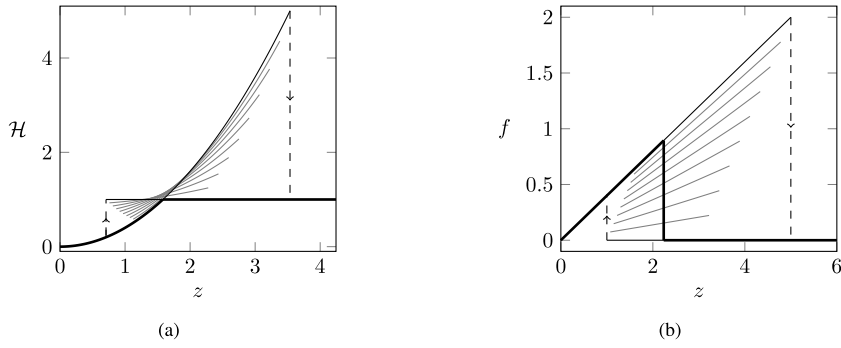


Fig. 2. Mechanical response of the model in a hard device. Solid black lines, global minimum, gray lines metastable states. Parameters are $N = 10$, $\lambda = 1$, $\lambda_f = 1$ and $l = \sqrt{2}$.

Here we first encounter one of our main nondimensional parameters

$$\Lambda = \lambda_f / \lambda_*. \tag{7}$$

where $\lambda_* = \lambda / (\lambda + 1)$ is the dimensionless effective stiffness of an individual breakable link. The synthetic parameter Λ can be perceived as inversely correlated with the system’s rigidity. It can be viewed as a measure of the overall ‘malleability’ of the structure.

The equilibrium values of x_i for the closed and open configurations are, respectively,

$$\hat{x}_0(k, z) = \frac{\lambda_f z}{1 - k/N + \Lambda}, \quad \hat{x}_{00}(k, z) = \frac{\Lambda z}{1 - k/N + \Lambda}. \tag{8}$$

Each value of k defines an equilibrium branch extending between the limits $(z_{inf}(k), z_{sup}(k))$. Due to the presence of the backbone, individual elements necessarily fail in sequence according to the value of their thresholds. Let $\bar{x}_i, i = 1, \dots, N$ be the ordered sequence of failure thresholds l_i : $\bar{x}_1 \leq \bar{x}_2 \leq \dots \leq \bar{x}_N$. In terms of the parameters \bar{x}_i we can formulate the constraints as $\hat{x}_0(k, z) < \bar{x}_k$ and $\hat{x}_{00}(k, z) > \bar{x}_k$. Therefore $\Lambda z_{inf} = \lambda_f z_{sup} = [1 - k/N + \Lambda] \bar{x}_k$. The special cases are the homogeneous configurations with $k = 0$, defined for $z \in (-\infty, z_{sup}(k = 0)]$ and with $k = N$, defined for $z \in [z_{inf}(k = N), \infty)$.

To analyze the stability of the obtained equilibrium states, we compute the Hessian of the energy $\tilde{H} = NH(x, y)$. We obtain

$$\underline{\underline{\mathcal{M}}} = \begin{pmatrix} \tilde{H}_1 & 0 & \dots & 0 & -\lambda \\ 0 & \ddots & \ddots & \vdots & \vdots \\ \vdots & \ddots & \ddots & 0 & \vdots \\ 0 & \dots & 0 & \tilde{H}_N & -\lambda \\ -\lambda & \dots & \dots & -\lambda & N(\lambda + \lambda_f) \end{pmatrix}, \tag{9}$$

where $\tilde{H}_i = \lambda + 1$ for $1 \leq i < N - k$ and $\tilde{H}_i = \lambda$ for $N - k \leq i \leq N$. The first N principal minors of \mathcal{M} are the product of diagonal terms \tilde{H}_i and are therefore always positive. The last principal minor is

$$\det(\underline{\underline{\mathcal{M}}}) = \prod_{i=1}^N \tilde{H}_i \sum_{i=1}^N \left(\lambda + \lambda_f - \frac{\lambda^2}{\tilde{H}_i} \right) \geq 0. \tag{10}$$

Therefore, all equilibrium configurations obtained above are stable. The unstable configurations must contain at least one element in the ‘spinodal’ state $x_i = l_i$.

To compute the equilibrium energy of the system we need to substitute into Eq. (2) the equilibrium values of the variables $\hat{y}(k, z)$ and $\hat{x}_i(k, z)$. We obtain

$$\mathcal{H}(k, z) = \frac{\lambda_f}{2} \frac{1 - k/N}{1 - k/N + \Lambda} z^2 + S_k. \tag{11}$$

where $S_k = N^{-1} \sum_{i=1}^k \bar{x}_i^2 / 2$ are the energies of the k disrupted bonds, and $S_0 = 0$. The tension–elongation relation for a microscopic state¹ characterized by the parameter k can be now written as

$$f(k, z) = \frac{\partial \mathcal{H}(k, z)}{\partial z} = \frac{\lambda_f (1 - k/N) z}{1 - k/N + \Lambda}. \tag{12}$$

Families of equilibrium branches parameterized by k can be computed explicitly, see an example with $N = 10$ and no disorder (homogeneous system) in Fig. 2.

¹ In our model, due to permutation invariance, the microscopic configuration is fully described by the number of open elements k .

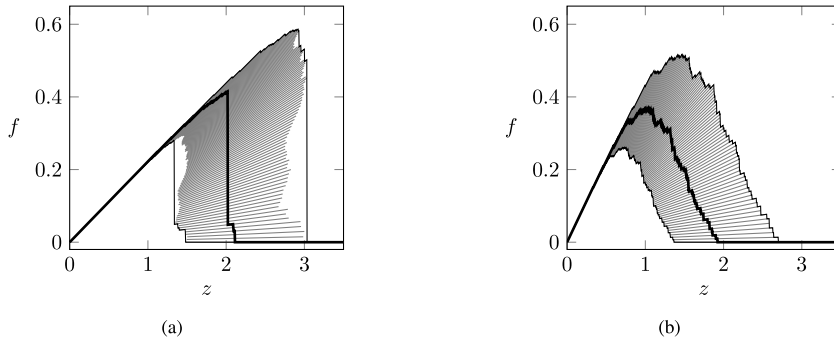


Fig. 3. Mechanical response of the model in a hard device. Solid black lines, global minimum; gray lines, metastable states; (a) $\Lambda = 0.8$, (b) $\Lambda \gg 1$. Parameters are $N = 100$, $\lambda = 1$ and thresholds follow a Weibull distribution with $\rho = 4$.

For a disordered system the effect of the parameter Λ is shown in Fig. 3 where $N = 100$ and the disorder is drawn from the one-parameter Weibull distribution, characterized by the probability density

$$p(x) = \rho x^{\rho-1} \exp(-x^\rho). \tag{13}$$

Here ρ will serve as our second most important dimensionless parameter, inversely correlated with the 'strength' of disorder.

2.1. Response strategies

Suppose now that the loading parameter z is changing quasi-statically. As a result the system will be almost always in the state of equilibrium. However, as we have seen above, there will be many equilibrium states at each value of the loading parameter z , including many locally stable states. Since the equilibrium branches of the energy \mathcal{H} are defined only for a finite range of values of the loading parameter z , it is still necessary to specify the internal dynamics of the system which ultimately controls the choice of a particular equilibrium branch and regulates the branch switching events. To have a maximally broad picture of possible mechanical responses we focus below on two extreme strategies predicting rather different mechanical responses (Puglisi and Truskinovsky, 2005).

Marginal stability. The first dynamic strategy can be viewed as the vanishing viscosity limit of the overdamped viscous dynamics (Selinger et al., 1991; Wang et al., 1991; Mielke and Truskinovsky, 2012). Under this protocol, which we will refer to as the *marginal stability* (MS) strategy/dynamics, the quasi-static loading maintains the system in a metastable state (local minimum of the energy) till it ceases to exist (till it becomes unstable). Then, during an isolated switching event, the system selects a new equilibrium branch using the steepest descent-type algorithm. This dynamic perspective can be viewed as a standard dogma in the macroscopic fracture mechanics of engineering structures.

Global minimum. The second dynamic strategy postulates that the system is always in the *global minimum* (GM) of the energy. It implies that at each value of the loading parameter z , the system is able to explore the energy landscape globally and minimize the energy absolutely. Physically, this branch selection strategy can be viewed as the zero temperature limit of the Hamiltonian equilibrium dynamics or as a response of a stochastic mechanical system exposed to a thermal reservoir (Francfort and Marigo, 1998; Bourdin et al., 2008; Efendiev and Truskinovsky, 2010). While for macroscopic engineering structures, the global energy minimization strategy does not look too realistic, at sufficiently small scales (encountered, for instance, in cells and tissues) it may be relevant. In such microscopic conditions and given that the observation is made over sufficiently long times, thermal fluctuations can be thought as exploring sufficiently large part of the phase space. In this sense the GM strategy should prove important for the description of low rate biomechanical phenomena where the energy scale of thermal fluctuations is comparable to the size of the energy barriers, see for instance, (Caruel and Truskinovsky, 2017).

2.2. Marginal stability strategy

To specify the MS response we first observe that each microscopic configuration exists in an extended domain of the loading parameter z and that the limiting points of these domains characterize the states of marginal stability. Define z_k as the marginal stability points for the branch with k broken elements. In such branch, $N - k$ elements are still holding the load, experiencing a common elongation \bar{x}_k (the threshold of the k 'th element). The force on the bundle is therefore $(N - k)\lambda(y - \bar{x}_k) = N\lambda_f(z_k - y)$, and if we eliminate y using Eq. (6) we obtain

$$z_k = \frac{\lambda + 1}{\lambda} \left[\left(1 - \frac{k}{N}\right) \frac{1}{\Lambda} + 1 \right] \bar{x}_k. \tag{14}$$

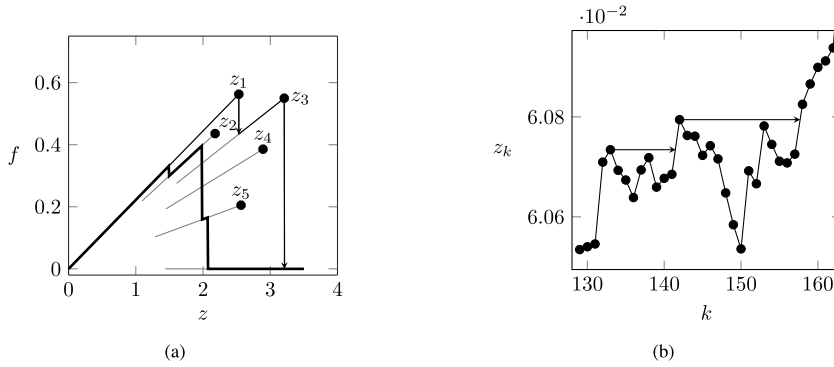


Fig. 4. (a) Load path for a system with $N = 5$. The thick line represent the GM response, while the thin line represent the MS response, in which the spinodal points z_k are given by Eq. (14) (b) Fluctuations of the spinodal points z_k for a bundle containing $N = 1000$ in the window with $129 \leq k \leq 162$. The first dashed black line illustrates an avalanche of size $\Delta = 9$ and the second line marks an avalanche of size $\Delta = 16$. Thresholds are drawn from the Weibull distribution (13) with $\rho = 4$.

We now recall that at an elongation x the expected number of broken bonds is $NP(x)$, thus only $N[1 - P(x)]$ bonds carry the total load, which means that the total force is $\bar{F}(x) = N[1 - P(x)]x$. The load per bond is then

$$\bar{f}(x) = [1 - P(x)]x. \tag{15}$$

The average displacement $\bar{z}(x)$ at elongation x can be assessed from Eq. (14) analytically in the limit $N \gg 1$. Then we can use the fact that the empirical cumulative distribution function $\hat{P}(x) = k/N$ is close in probability to the cumulative distribution function $P(x)$. Moreover, the order statistics of \bar{x}_k can be then approximated by $P^{-1}(k/N)$. Then $\bar{x}_k \rightarrow P^{-1}(P(x)) = x$ and Eq. (14) can be approximated by

$$\bar{z}(x) = \frac{\lambda + 1}{\lambda} \left[[1 - P(x)] \frac{1}{\Lambda} + 1 \right] x. \tag{16}$$

If we combine Eqs. (15) and (16) using the elongation x as a parameter, we can compute the average force–elongation response $\bar{f} = \bar{f}(\bar{z})$.

In Fig. 4(a) we illustrate the fine structure of a typical MS force–elongation curve using as an example a small system with $N = 5$. We see that in this example, after the first element breaks, the system skips one metastable branch before it reaches the stable one, producing an avalanche of size two. As the load increases further, the next marginal stable endpoint z_3 is reached, and the system jumps to the new configuration, breaking at once two more elements and thus exhibiting an avalanche of size three. We can conclude that when the thresholds are disordered, the MS response is characterized by a series of intermittent jumps, see an example with $N = 100$ in Fig. 3(b). This figure suggests that small Λ favors macroscopic fracture (collective breaking) while large Λ produces sequential uncoordinated microfracturing as the complete synchronization is, in this case, more easily compromised by the disorder.

2.3. Global minimization strategy

If we adopt the GM dynamics we obtain rather different response. It can be reconstructed by comparing the energies of different equilibrium configurations at a given value of z and choosing the configuration that minimizes the energy. In contrast to the homogeneous case, the presence of the stochastic term S_k makes it challenging to define analytically the transitions points z_k separating different energy minimizing branches. The explicit results can be obtained in a simple form only at $N \gg 1$ when one can use convenient properties of order statistics.

Indeed, in the limit $N \rightarrow \infty$ we can approximate the sum in the definition of S_k by an integral

$$S_k = \frac{1}{N} \sum_{i=0}^k \frac{\bar{x}_i^2}{2} \approx \int_{\bar{x}_1}^{\bar{x}_k} \frac{x^2}{2} dP(x), \tag{17}$$

where we used that $k/N \rightarrow P(\bar{x}_k)$, and identified the increment $dP(x)$ with $1/N$. The ensuing asymptotic expression for the energy, Eq. (11) can be written in the form

$$H(x, z) = \frac{\lambda_f(1 - P(x))}{1 - P(x) + \Lambda} \frac{z^2}{2} + \int_0^x p(x') \frac{x'^2}{2} dx'. \tag{18}$$

From the equilibrium equation $\partial H(x, z)/\partial x = 0$ we obtain the desired relation $\bar{z}(x)$.

$$\bar{z} = (1 - P(x) + \Lambda) \frac{x}{\sqrt{\lambda_f \Lambda}}. \tag{19}$$

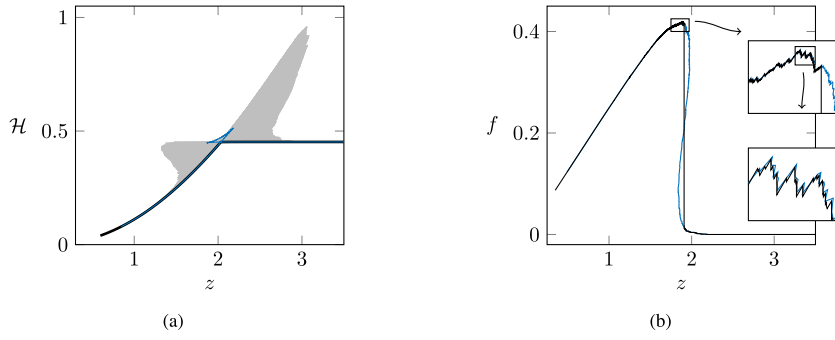


Fig. 5. (a) Energy–elongation relation, (b) force–elongation. In (a) the light gray region corresponds to the metastable states; (a) and (b): the black thick line is the load path following the global minimum of the energy, the blue curve is the global minimum path as predicted by Eq. (20). Parameters: $\rho = 5$, $\lambda = 1$, $\lambda_f = 0.4$, and $N = 500$.

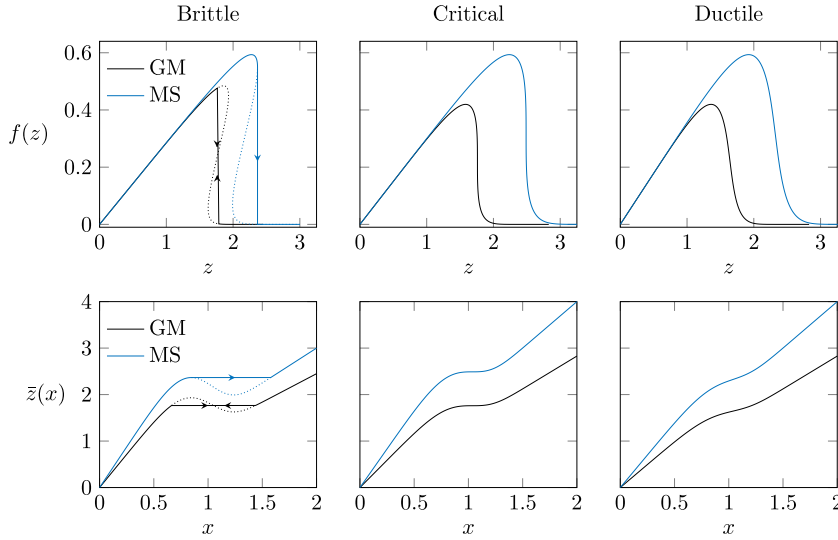


Fig. 6. First row: force elongation, second row: external elongation as a function of internal variable x . The blue curves correspond to the unbinding path under the MS dynamics; The black curves correspond to the GM dynamics.

To see how relevant such approximation may be at finite N we rewrite the asymptotic relation (19), in a discrete form, by assuming that the continuous variable x takes only discrete values \bar{x}_k

$$z_k = \left(1 - \frac{k}{N} + \Lambda\right) \frac{\bar{x}_k}{\sqrt{\lambda_f \Lambda}}. \quad (20)$$

We can then substitute (20) into (11) and reconstruct the GM response. In Fig. 5(b), we compare for the case $N = 500$ the results of direct numerical minimization of the energy with the theoretical prediction based on (20). The overall agreement is very good, even at finer scales, even though, the approximate theory does not capture every single fluctuation.

The $N \rightarrow \infty$ limits for MS and GM paths are compared in Fig. 6. It illustrates the important role played by the parameter Λ . At a fixed disorder, the system fractures gradually when Λ is large, and we identify this regime with *ductile* fracture. Instead, at small values of Λ we observe a finite abrupt discontinuity and associate such regimes with *brittle* fracture. Since our averaged force–elongation curves are obtained from the parametric equations for $f(x)$ and $z(x)$, whenever we have a discontinuity in $f(z)$ we also have a discontinuity in $z(x)$. In other words, if at a fixed elongation z , there are multiple configurations satisfying (19) or (16), we deal with the brittle regime.

2.4. Brittle to ductile transition

To distinguish between brittle and ductile responses in the framework of MS dynamics, we need to check if there are roots of the equation $\partial \bar{z}(x)/\partial x = 0$, where $\bar{z}(x)$ is given by Eq. (16), corresponding to a local maximum. If there is such a root $x = x_*$ it solves

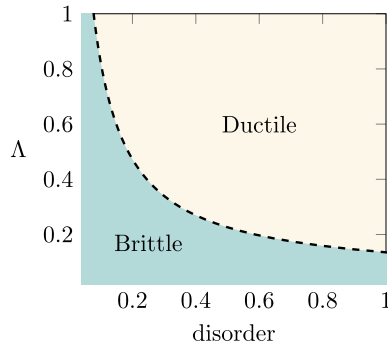


Fig. 7. The phase diagram constructed based on Eq (23). We used the variance of the Weibull distribution, $\text{Var}(\rho) = \Gamma(1 + 2/\rho) - [\Gamma(1 + 1/\rho)]^2$, as the measure of the 'strength' of disorder. The 'malleability' parameter Λ is viewed as inversely correlated to the system's rigidity. A closely related but differently parameterized empirical phase diagram has been recently obtained in (David et al., 2021).

the equation

$$1 - P(x) - p(x)x + \Lambda = 0. \tag{21}$$

The existence of solutions of Eq. (21) is then a fingerprint of collective debonding events, see Fig. 6. The critical regime, separating brittle from ductile responses, corresponds to the parameter choice when the solution of Eq. (21) is an inflection point. Such $x = x_c$ should also solve $\partial^2 \bar{z}(x)/\partial x^2 = 0$, which can be rewritten as

$$-2p(x) - p'(x)x = 0. \tag{22}$$

To summarize, the critical manifold in the space of parameters can be found by eliminating x from Eqs. (21) and (22).

Note next that whenever the system is brittle under the MS dynamics, it is also brittle under the GM dynamics. However, in the latter case the system does not reach the maximum on the curve $\bar{z}(x)$ (spinodal point), because the energy minimizing configuration is switched earlier and the point of collective debonding should be chosen instead by the Maxwell construction, see Fig. 6. According to Eq. (19), the condition for the local maximum of $\bar{z}(x)$ is again given by (21). Similarly, the condition for an inflection point is again (22). Hence, the critical manifold, separating brittle from ductile regimes in the space of parameters, is independent of the loading protocol.

The location of the boundary separating brittle and ductile regimes depends on the strength of the disorder (the parameter ρ for the Weibull distribution) and on the dimensionless parameter Λ which we interpret as a measure of the structural rigidity of the system (Merkel et al., 2019; Vermeulen et al., 2017; Crapo, 1979; Kim et al., 2019). When Λ is large, meaning that either λ_f is large or λ is small, individual breakable elements interact weakly. In fact, the limit $\Lambda \rightarrow \infty$ can be associated with the jamming threshold (isostatic point) beyond which the rigidity is completely lost (Goodrich et al., 2014). Instead, when $\Lambda \rightarrow 0$ the system can be viewed as over-constrained (Driscoll et al., 2016). In some sense, the dimensionless parameter Λ is similar to the effective Poisson's ratio ν , which is by itself positively correlated with the ratio κ/μ where κ is the effective bulk modulus and μ is the effective shear modulus. Both these dimensionless parameters decrease with increased connectivity of the lattice/network, which diminishes fracture toughness and favors brittleness. Instead they increase with denser packing, which enhances fracture toughness and facilitates ductility (Greaves et al., 2011; Richard et al., 2021; Deng and Shi, 2018; Østergaard et al., 2019)

To illustrate these results, we use again our one-parameter Weibull distribution of thresholds, characterized by a single shape parameter ρ which can be viewed as inversely proportional to the variance of the disorder. One can show that in this case the boundary between the brittle and ductile regimes is given by the explicit relation

$$\Lambda = \rho \exp(-1/\rho - 1). \tag{23}$$

According to (23) ductility can be achieved by decreasing the degree of interaction/connectivity among individual binders measured by any rigidity measure negatively correlated, say, inversely proportional (Borja da Rocha and Truskinovsky, 2020), to our parameter Λ . Indeed, the bigger the Λ , the less sensitive the binders are to a change in the configuration of their neighbors. Since disorder tends to desynchronize the bonds, Eq. (23) predicts a transition from brittle response (correlated microfailure) at small disorder to ductile response (uncorrelated microfailure) at large disorder. The corresponding phase diagram in the space rigidity–disorder is presented in Fig. 7.

3. Empirical avalanche distribution

So far we were mostly concerned with the averaged behavior, neglecting fluctuations. Now, we change focus and turn to the statistics of avalanches as the system is quasi-statically loaded in the hard loading device.

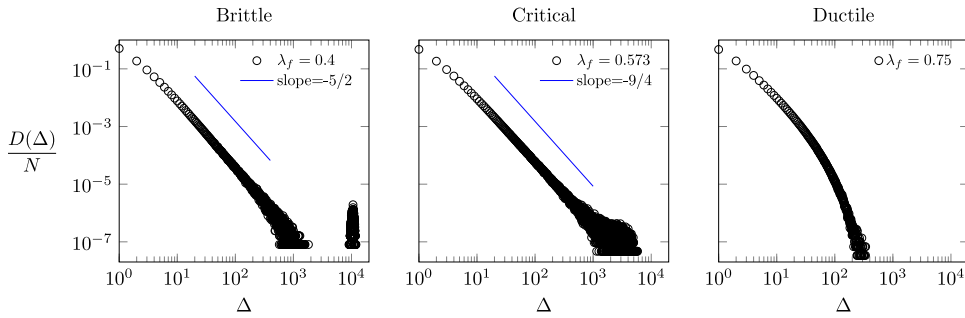


Fig. 8. Avalanche distribution $p_a(\Delta) = D(\Delta)/N$ where $D(\Delta)$ is the number of avalanches with the size Δ . We used MS protocol for the system with $N = 20000$, $\lambda = 1$ and thresholds following a Weibull distribution with $l = 1$ and $\rho = 4$. The distribution is averaged over 10000 realizations of the disorder.

3.1. Marginal stability strategy

The occurrence of avalanches under MS dynamics can be predicted if we know the sequence of external elongations $\{z_k\}$, defined as the instability points for the branches with $k - 1$ broken elements and given by (14). For an avalanche of size Δ to start when the k th fiber is about to break, two conditions must be satisfied. The first condition is called the *forward condition* and it states that $\Delta - 1$ fibers must fail after the breaking of the k th fiber. The second condition, called the *backwards condition*, ensures that the avalanche starts indeed with the breaking of the k th fiber and it is not a part of a bigger one. These conditions will be used in our numerical experiments in the analytical form

1. $z_{k+j} \leq z_k$, for $j = 1, 2, \dots, \Delta - 1$ and $z_{k+\Delta} > z_k$. (forward condition)
2. $z_j \leq z_k$, for all $j < k$, (backwards condition)

Numerical experiments. To reveal the response of the system we conducted a series of numerical experiments varying the parameters of the system and the realizations of disorder. Our experiments unveiled the existence of the two main fracture regimes (brittle and ductile). They also showed that the range of scaling blows up at the boundary between the two regimes suggesting criticality.

More specifically we were interested in the expected number of bursts of a particular size Δ . In Fig. 8, we present the numerically computed avalanche distribution $p_a(\Delta)$ in the brittle ($\lambda_f = 0.4$), critical ($\lambda_f = 0.573$) and ductile ($\lambda_f = 0.75$) regimes under the MS dynamics. In the brittle regime, we found the power law type distribution with

$$p_a(\Delta) \sim \Delta^{-\alpha}.$$

The exponent $\alpha = 5/2$ turned out to be the same one as the one found in the classical force-controlled FBM (Hansen et al., 2015; Hansen and Hemmer, 1994; Hemmer and Hansen, 1992; Kloster and Hemmer, 1997; Pradhan et al., 2010). However, the obtained distribution is only super-critical because of the presence of the peak, representing system-size events.

In the critical regime, we also observed the power law distribution but now with the exponent $\alpha = 9/4$, which was not known in the classical FBM. Finally, in the ductile regime, the distribution is of power law type only for very small events but then exhibits an exponential decay suggesting Gaussian distribution.

3.2. Global minimum strategy

Under the GM dynamics the response reduces to the global minimization of the energy (11). Suppose that an avalanche event happens at an elongation $z = \zeta$, in a state where the maximally stable configuration has k bonds that are broken. If Δ further bonds are broken in the avalanche, the next stable configuration must satisfy $\mathcal{H}(\zeta, k) = \mathcal{H}(\zeta, k + \Delta)$. Moreover, we have to ensure that the configurations k and $k + \Delta$ are indeed the ones that minimize the energy at ζ . Thus, the energy of the configurations between the two states $k, k + \Delta$ have to be greater than $\mathcal{H}(\zeta, k)$, which means $\mathcal{H}(\zeta, k) < \mathcal{H}(\zeta, k + j)$, with $j = 1, \dots, \Delta - 1$. Let $E_i(\zeta) \equiv \mathcal{H}(z = \zeta, i)$ be the sequence of the energies of the system at fixed elongation ζ corresponding to different configurations i . The conditions for the avalanche of size Δ starting at k can be then formulated in terms of $E_i(\zeta)$ as,

1. $E_k(\zeta) < E_{k+i}(\zeta)$, for $i = 1, \dots, \Delta - 1$ and $E_k(\zeta) \geq E_{k+\Delta}(\zeta)$ (forward condition)
2. $E_k(\zeta) < E_j(\zeta)$, for $j < k$ (backwards condition)

Numerical experiments. Using these conditions we can obtain numerically the force–elongation curve and study the statistics of avalanches. Our numerical experiments, summarized in Fig. 9, show that the overall structure for the breaking sequence along the GM path is similar to the one we obtained in the case of the MS dynamics. When the k 'th bond is about to break to ensure the global minimization of the energy, the elongation per fiber is given by Eq. (20). Note that Eq. (20) was obtained for $N \gg 1$. This means that for large clusters we can compute the avalanche distribution in a similar way as in the out of equilibrium case. Moreover, one should then expect that the statistical features of equilibrium (GM) and nonequilibrium (MS) avalanche distributions would

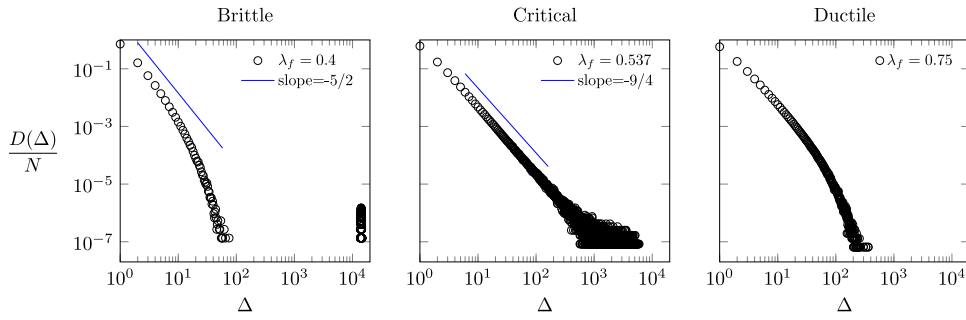


Fig. 9. Avalanche distribution $p_\sigma(\Delta) = D(\Delta)/N$ where $D(\Delta)$ is the number of avalanches with the size Δ . We used the GM protocol for the system with $N = 20000$, $\lambda = 1$ and thresholds following a Weibull distribution with $l = 1$ and $\rho = 4$. The distribution is averaged over 10000 realizations of the disorder.

be the same. Our numerical experiments show that, indeed, the equilibrium avalanche statistics in the critical and ductile regimes are identical to the ones in the out-of-equilibrium system. However, as we can see in Fig. 9, the statistics for the brittle regime are not the same. While in the case of MS dynamics we see a power law with a peak, in the global minimization response we see a power law with exponential decay followed by a peak. The reason is that in the latter case the system collectively fractures before it reaches the state where the stiffness diverges.

Our numerical experiments suggested the direction of the development of the analytical theory which is presented in the next sections. Such theory must justify the existence of the two different fracture regimes (brittle and ductile) and it is expected to show that equilibrium and non-equilibrium exponents agree. It should also be able to show that the range of scaling blows up at the boundary between the two regimes suggesting full scale criticality on the BDT boundary.

4. Avalanche as a random walk

To justify analytically the empirical avalanche distributions shown in Figs. 8 and 9 we first show that the process of propagating fracture can be represented by a (biased) random walk, see for the initial insights (Sornette, 1992; Pradhan et al., 2010; Sornette, 2006). Each step of the random walk represents the breaking of a single element, and therefore such random walk has a constant step size. Because of the random nature of the thresholds \bar{x}_k an avalanche event can be seen as a return (first passage) time problem for a random walk. To compute the probability of an avalanche of size Δ happening at configuration k is then equivalent to computing the probability of the random walk z_k return after Δ steps.

MS dynamics. To compute the probability of an avalanche of size Δ along the MS path which starts with the breaking of the k th element we need to know the probability distribution of the *small* length increments $\delta z(x) = z_{k+1} - z_k$, where we assumed that at the point of instability $z_k = z$ the configuration is $\bar{x}_k = x$. In the limit $N \gg 1$ it will be more convenient to deal with the *finite* length increments (jumps) $[[Z]] = N \delta z(\lambda/(\lambda + 1))\Lambda$. We can use (14) to write

$$[[Z]] = (1 - k/N + \Lambda)N\delta x - x, \quad (24)$$

where $\delta x = \bar{x}_{k+1} - x$ are the *small* increments of the threshold values. The probability distribution of \bar{x}_{k+1} , under condition that $\bar{x}_k = x$, can be written as

$$\rho(\bar{x}_{k+1}) = (N - k) \left[\frac{1 - P(\bar{x}_{k+1})}{1 - P(x)} \right]^{N-k-1} \frac{p(\bar{x}_{k+1})}{1 - P(x)}. \quad (25)$$

Using (24) and the fact that $N \gg 1$ we can now rewrite (25) as the probability distribution $\rho([[Z]])$. Indeed, in the limit $N \rightarrow \infty$, we have $k/N \approx P(x)$, $p(\bar{x}_{k+1}) \approx p(x)$. Moreover, since $\bar{x}_k \rightarrow P^{-1}(k/N)$, we can use the approximation $\bar{x}_{k+1} - \bar{x}_k \rightarrow P^{-1}((k+1)/N) - P^{-1}(k/N) \sim 1/N$. Then, given that $\delta x \ll x$, we can write

$$\left[\frac{1 - P(x + \delta x)}{1 - P(x)} \right]^{N-k-1} \approx \exp \left[-p(x) \left(\frac{[[Z]] + x}{1 - P(x) + \Lambda} \right) \right]. \quad (26)$$

Hence

$$\rho([[Z]]) = \begin{cases} \frac{p(x)}{1 - P(x) + \Lambda} \exp \left[-\frac{p(x)}{1 - P(x) + \Lambda} ([[Z]] + x) \right], & [[Z]] + x \geq 0, \\ 0, & [[Z]] + x < 0. \end{cases} \quad (27)$$

This distribution defines the asymmetric random walk with the average step,

$$\langle [[Z]] \rangle = (1 - P(x) + \Lambda - x p(x))/p(x), \quad (28)$$

which is non-zero, except at the critical or spinodal points, see (21). To characterize the random walk fully, we would also need to know the variance

$$\sigma_{[[Z]]}^2 = (1 + \Lambda - P(x))^2/p(x)^2. \quad (29)$$

Then the step bias of the ensuing random walk is

$$b \equiv \frac{\langle [Z] \rangle}{\sigma_{[Z]}} = 1 - \frac{x p(x)}{1 + \Lambda - P(x)} = 1 - g(x), \tag{30}$$

where

$$g(x) = \frac{p(x)x}{1 - P(x) + \Lambda}. \tag{31}$$

Note that $b = 0$ in spinodal and critical regimes, where $g(x) = 1$ (see Eq. (21)), and $b > 0$ otherwise.

GM dynamics. Similarly, in the context of GM dynamics we can consider the sequence E_k as a biased random walk with unitary step sizes. As before, we will focus on the computation of the asymptotic probability distribution for the *finite* energy increments $[[E]](x) = N(E_{k+1}(x) - E_k(x))$, where E_k corresponds to $\bar{x}_k = x$. Given that $N \gg 1$ we can approximate x using Eq. (20) and then use Eq. (11) to write,

$$[[E]] = -\frac{1}{1 - (1 - k/N + \Lambda)^{-1} N^{-1}} \frac{x^2}{2} + \frac{\bar{x}_{k+1}^2}{2} \approx -\left[1 + \frac{1}{(1 - k/N + \Lambda)N}\right] \frac{x^2}{2} + \frac{\bar{x}_{k+1}^2}{2}. \tag{32}$$

Next, we introduce a new random variable $\xi = x^2/2$ with cumulative distribution $F(\xi)$ and probability density $f(\xi)$. Given that $\xi_k = \xi$, the distribution function for ξ_{k+1} can be written as

$$\rho(\xi_{k+1}) = (N - k) \left[\frac{1 - F(\xi_{k+1})}{1 - F(\xi)} \right]^{N-k-1} \frac{f(\xi_{k+1})}{1 - F(\xi)}. \tag{33}$$

We can then use (32) to obtain the probability density $\rho([[E]])$. In the limit $N \rightarrow \infty$ we can write

$$\rho([[E]]) = (N - k) \left[\frac{1 - F(\xi + \delta\xi)}{1 - F(\xi)} \right]^{N-k-1} \frac{f(\xi_{k+1})}{1 - F(\xi)} \tag{34}$$

and, since the increments $\delta\xi = N^{-1}[[E]] + [(1 - k/N + \Lambda)N]^{-1}\xi \sim 1/N$ are *small* $\delta\xi \ll \xi$, we can use the approximation

$$\left[\frac{1 - F(\xi + \delta\xi)}{1 - F(\xi)} \right]^{N-k-1} \approx \exp \left[-f(\xi) \left([[E]] + \frac{\xi}{1 - F(\xi) + \Lambda} \right) \right]. \tag{35}$$

Finally, using the fact that $f(\xi_{k+1}) \approx f(\xi)$, we obtain the desired distribution

$$\rho([[E]]) = \begin{cases} N f(\xi) \exp \left[-f(\xi) \left([[E]] + \frac{\xi}{1 - F(\xi) + \Lambda} \right) \right], & [[E]] + \frac{\xi}{1 - F(\xi) + \Lambda} \geq 0, \\ 0, & [[E]] + \frac{\xi}{1 - F(\xi) + \Lambda} < 0. \end{cases} \tag{36}$$

Since $\bar{x}_i \geq 0$, the probability distributions for $\xi = x^2/2$ can be expressed through the known distribution for x , in particular, $F(\xi) = P(x)$, and $f(\xi) = \frac{2}{x} p(x)$. Therefore we can rewrite (36) as

$$\rho([[E]]) = \begin{cases} N \frac{2p(x)}{x} \exp \left[-\frac{2p(x)}{x} \left([[E]] + \frac{x^2/2}{1 - P(x) + \Lambda} \right) \right], & [[E]] + \frac{x^2/2}{1 - P(x) + \Lambda} \geq 0, \\ 0, & [[E]] + \frac{x^2/2}{1 - P(x) + \Lambda} < 0. \end{cases} \tag{37}$$

For the ensuing random walk we can now compute the mean

$$\langle [[E]] \rangle = x(1 - g(x))/(2N p(x)), \tag{38}$$

and the variance

$$\sigma_{[[E]]}^2 = x^2/(2N p(x))^2. \tag{39}$$

The corresponding step bias is then

$$b \equiv \frac{\langle [[E]] \rangle}{\sigma_{[[E]]}} = 1 - g(x), \tag{40}$$

which is exactly the same expression as in the case of MS dynamics.

Given that we mapped avalanches on one dimensional random walks with constant step size, the statistics of avalanches can be obtained from the solution of the general *first passage* time problem for such stochastic processes (Metzler et al., 2014). Our return problem is then equivalent of the first passage problem with the “return point” chosen to coincide with the origin.

Indeed, consider an abstract 1D random walk of this type and denote the probability of taking a step in the positive direction by p and in the negative direction by $q = 1 - p$. For such random walk, the average advance is

$$\langle [r] \rangle = p - q, \tag{41}$$

the standard deviation is

$$\sigma_{[r]} = \sqrt{4pq}. \tag{42}$$

Then for the step bias relative to the standard deviation, we obtain

$$\frac{\langle [r] \rangle}{\sigma_{[r]}} = \frac{p - q}{\sqrt{4pq}}. \tag{43}$$

For a general random walk, satisfying the forward condition is equivalent to solving a special case of the gambler’s ruin problem in the interval $(0, \infty)$ with an absorbing barrier at 0. The amount of steps before the return is exactly the avalanche size Δ .

To find the avalanche distribution, we define the probability $\psi_{1,n}$ that our general random walk initiated at $r = 1$ returns at $r = n$. The solution of this classical problem is known (Feller, 1968)

$$\psi_{1,n} = \frac{1}{n} \binom{n}{(n+1)/2} p^{(n-1)/2} q^{(n+1)/2}. \tag{44}$$

We now assume that $n \gg 1$ and associate with n the avalanche of size Δ . Then the avalanche distribution is $p \psi_{1,\Delta}$, where the p factor ensures that the first step is in the positive direction. We obtain

$$p \psi_{1,\Delta} \approx \sqrt{1/2\pi} \Delta^{-3/2} (4pq)^{\Delta/2} \sqrt{p/q}. \tag{45}$$

We can now associate our general random walk with the discrete failure process under either MS or GM protocols. We recall that the relative bias is the same under both conditions, and hence we can use the identification

$$\frac{p - q}{\sqrt{4pq}} = \frac{\langle [E] \rangle}{\sigma_{[E]}} = \frac{\langle [Z] \rangle}{\sigma_{[Z]}} = 1 - g(x). \tag{46}$$

Since we are mainly interested in the case of *small* bias b , as the main avalanche statistics is acquired near either spinodal or critical points, we can write $p = (1 + b)/2$ and $q = (1 - b)/2$. Therefore

$$\frac{p - q}{\sqrt{4pq}} = \frac{b}{1 - b^2} \approx b. \tag{47}$$

We have thus used the forward condition. The backwards condition states that the zero level is not reached before the end of the avalanche. Under the assumption that $n \gg 1$ this means that the time-reversed process never returns. The probability of no return for such random walk is (Feller, 1968; Hansen et al., 2015)

$$p_{bc} = |p - q| = b. \tag{48}$$

Bringing these results together, we can present the probability of having an avalanche of size Δ in the form

$$\Psi(\Delta) = p \psi_{1,\Delta} p_{bc} = \frac{1}{\sqrt{2\pi}} \Delta^{-3/2} b e^{\log(1-b^2)\Delta/2} \sqrt{\frac{1+b}{1-b}} \approx \frac{1}{\sqrt{2\pi}} \Delta^{-3/2} b e^{-b^2\Delta/2}, \tag{49}$$

where we used the small bias approximations $\log(1 - b^2) \approx -b^2$, and $\sqrt{(1 + b)/(1 - b)} \approx 1$.

In both MS and GM dynamics, we deal with cases where the parameter b depends on the value of the elongation x at which breaking begins. To account for this parametric dependence we use the notation $\Psi(\Delta; x)$. Since the number of elements with thresholds in $(x, x + dx)$ is $Np(x)dx$, the number of avalanches of size Δ starting inside $(x, x + dx)$ is $\Psi(\Delta; x)Np(x)dx$. Then the distribution of avalanches in the range (x_i, x_s) , close to either spinodal or critical point is

$$p_a(\Delta) \equiv \frac{D(\Delta)}{N} = \frac{1}{\sqrt{2\pi}} \Delta^{-3/2} \int_{x_i}^{x_s} \phi(x) e^{-h(x)\Delta} dx, \tag{50}$$

where $\phi(x) = [1 - g(x)]p(x)$ and $h(x) = [1 - g(x)]^2$. The distribution (50) has the same structure as the one obtained in the classical fiber bundle model loaded in a soft device (Hansen et al., 2015; Hemmer and Hansen, 1992; Halász and Kun, 2010). The new element is the appearance of the parameter $\Lambda = \lambda_f(\lambda + 1)/\lambda$, which can differentiate between brittle and ductile behaviors. Numerical simulations, Figs. 8 and 9, suggest different exponents in different ranges of Λ and our asymptotic analysis of Eq. (50) in the next section will reveal the origin of these differences.

5. Avalanche distribution: asymptotic results

Since both MS and GM random walks have the same bias $b(x)$, the corresponding asymptotics for the avalanche distribution can be expected to be the same in the critical and the ductile regimes. In the brittle regime, the MS and GM dynamics can be expected to produce different types of system spanning events, spinodal and equilibrium (Maxwellian), respectively, and therefore these two cases would have to be treated separately.

Using the fact that Δ is large, we can approximate the integral in Eq. (50) using Laplace’s method around the global minimum of the function $h(x)$. If the minimum at, say $x = x_0$, exists, then for large Δ the main contribution to the integral will come from the vicinity of x_0 . To find this point we need to solve the equation $h'(x) = 2g'(x)(1 - g(x)) = 0$. There are two classes of solutions of this equation corresponding to either $g(x_0) = 1$ or $g'(x_0) = 0$. This leads to three possibilities,

1. $g(x_0) \neq 1$ and $g'(x_0) = 0$,
2. $g(x_0) = 1$ and $g'(x_0) = 0$,

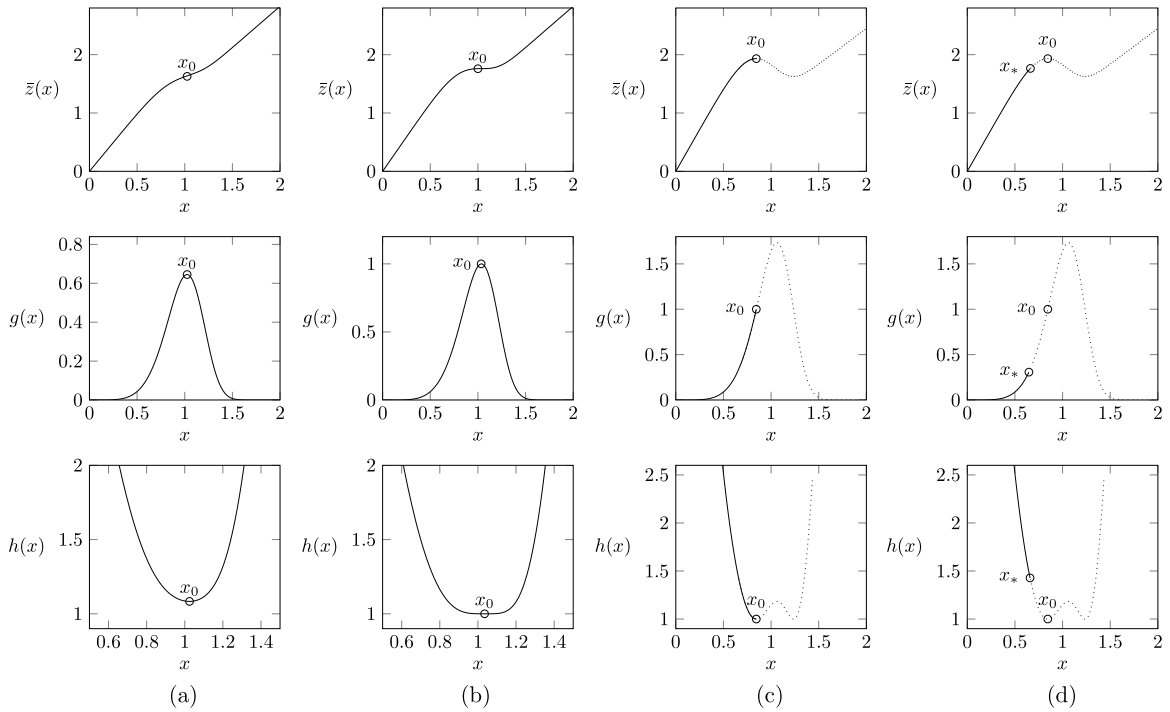


Fig. 10. Behavior of the functions $z(x)$, $g(x)$ and $h(x)$ when the system is in: (a) the ductile regime; (b) the critical regime; (c) the brittle regime under the MS dynamics; (d) the brittle regime under the GM dynamics.

3. $g(x_0) = 1$ and $g'(x_0) \neq 0$.

These three types of solutions produce our three regimes: ductile, critical and brittle, respectively.

Indeed, the condition $g(x_0) = 1$ is equivalent to,

$$p(x_0)x_0 = 1 - P(x_0) + A, \tag{51}$$

which is our condition of brittleness based on the averaged description, see Eq. (21). The condition $g'(x_0) = 0$ can be rewritten as $2/x_0 + p'(x_0)/p(x_0) = 0$, and is therefore equivalent to the condition $\partial^2 \bar{z}(x)/\partial x^2 = 0$ indicating an inflection point on the $z(x)$ curve. In the absence of the minimum of $h(x)$, we have $g(x_0) \neq 1$, and then the condition $g'(x_0) = 0$ characterizes the ductile response. Finally, when both conditions $g(x_0) = 1$ and $g'(x_0) = 0$ are met, we have critical behavior. While in the case of MS dynamics all three of these possibilities can be realized, in the brittle regime the GM response is characterized by a (Maxwell) jump taking place before the spinodal point (51) is reached. All these different possibilities are illustrated in Fig. 10.

5.1. Ductile behavior

If the minimum of $h(x)$ is defined by the conditions $g'(x_0) = 0$ and $g(x_0) \neq 1$, we can write,

$$h(x) \approx [1 - g(x_0)]^2 + g''(x_0)[1 - g(x_0)](x - x_0)^2. \tag{52}$$

Then the application of the saddle-point approximation to (50) gives

$$p_a(\Delta) = \frac{1}{\sqrt{2\pi}} \Delta^{-3/2} [1 - g(x_0)] p(x_0) e^{-\Delta[1 - g(x_0)]^2} \sqrt{\frac{2\pi}{\Delta |h''(x_0)|}} \propto \Delta^{-2} e^{-\Delta[1 - g(x_0)]^2}. \tag{53}$$

While here the asymptotic behavior of the distribution is fully dominated by an exponential cut-off, the exponent value -2 can be still read of the empirical diagrams shown in Figs. 8 and 9 for ductile behavior.

5.2. Critical behavior

The next special case is when simultaneously $g(x_0) = 1$ and $g'(x_0) = 0$. Since then $h''(x_0) = 0$, higher order terms have to be included into the expansion of the function $h(x)$. The third derivative term also vanishes, $h'''(x_0) = 0$, and therefore the Taylor

expansion of $h(x)$ starts with the fourth order term $h(x) \approx (h^{(4)}(x_0)/4!)(x - x_0)^4$, where $h^{(4)}(x_0) = 3g''(x_0)^2$. Moreover, we can write $\phi(x) \approx (\phi''(x_0)/2)(x - x_0)^2$, with $\phi''(x_0) = -p(x_0)g''(x_0)$, which allows us to re-write the integral (50) as

$$p_a(\Delta) = \frac{\Delta^{-3/2}}{\sqrt{2\pi}} \int_{x_i}^{x_0} -p(x_0)g''(x_0)(x - x_0)^2 e^{-\Delta \frac{3g''(x_0)^2}{4!}(x-x_0)^4} dx. \tag{54}$$

Finally, performing the integration explicitly we obtain

$$p_a(\Delta) = \frac{\Delta^{-3/2}}{\sqrt{2\pi}} \frac{p(x_0)g''(x_0)}{4 \left(\Delta \frac{3g''(x_0)^2}{4!}\right)^{3/4}} \Gamma\left(\frac{3}{4}, \Delta \frac{3g''(x_0)^2}{4!}(x - x_0)^4\right) \Big|_{x_i}^{x_s}, \tag{55}$$

where we introduced the incomplete gamma function $\Gamma(s, x) = \int_x^\infty t^{s-1} e^{-t} dt$. The lower limit of the integral does not contribute when Δ is large and we can write the following asymptotic representation for the avalanche size distribution

$$p_a(\Delta) \sim \Delta^{-\alpha}, \tag{56}$$

where $\alpha = 9/4$. Note that such critical regimes in the case of MS and GM dynamics are characterized by the same exponent and therefore belong to the same universality class. Similar 'super universality' for the random-field Ising model was shown in (Balog et al., 2014).

5.3. Brittle behavior

MS dynamics. Suppose now that x_0 solves the equation $g(x_0) = 1$ which is precisely Eq. (21), identifying the brittle regime. The avalanches must be counted till the point x_0 where the system undergoes a system size macroscopic failure. We can then expand the function $h(x)$ to obtain $h(x) \approx \frac{h''(x_0)}{2}(x - x_0)^2$, where $h''(x_0) = [g'(x_0)]^2$. Since $g(x_0) = 1$ we also have $\phi(x_0) = [1 - g(x_0)] p(x_0)/g(x_0) = 0$, so in addition to $h(x)$ we can also expand $\phi(x)$ to obtain $\phi(x) \approx -g'(x_0)p(x_0)(x - x_0)$. Using these results we can approximate the integral (50) by

$$p_a(\Delta) = \frac{\Delta^{-3/2}}{\sqrt{2\pi}} \int_{x_i}^{x_0} g'(x_0)p(x_0)(x_0 - x) e^{-\Delta \frac{g'(x_0)^2}{2}(x-x_0)^2} dx. \tag{57}$$

Since we are in the brittle regime and the avalanches are counted up to $x = x_0$ we can compute the Gaussian integral explicitly

$$p_a(\Delta) = \frac{\Delta^{-5/2}}{\sqrt{2\pi}} \frac{g'(x_0)p(x_0)}{[g'(x_0)]^2} e^{-\Delta \frac{g'(x_0)^2}{2}(x-x_0)^2} \Big|_{x_i}^{x_0}. \tag{58}$$

At large Δ the lower limit gives a vanishing contribution, which allows us to write the final asymptotic formula for the avalanche size distribution in the form $p_a(\Delta) \sim \Delta^{-\alpha}$, with $\alpha = 5/2$. As we have already mentioned before, this value of the exponent α already appeared in the studies of the classical FBM loaded in the soft device (Hemmer and Hansen, 1992) and was associated with spinodal criticality (Alava et al., 2006). Our model is an extension of this earlier model in the sense that the soft device case can be obtained in the limit $\Lambda \rightarrow 0$. We can then conclude that the scaling in the brittle regime is also of the spinodal type. Note, however, that such spinodal regime is not critical but super-critical in view of the presence of the system-size spanning events.

GM dynamics. While the analysis presented above of the brittle regime is valid for the case of MS dynamics, it cannot be automatically extended to the case of GM dynamics. Indeed, recall that the condition $g(x_0) = 1$, which coincides with Eq. (21), states that the averaged response curve $z(x)$ has a (local) maximum. However, we know that along the GM path the system size failure takes place before the point x_0 . In particular, in the GM instability point $x_* < x_0$, where the corresponding Maxwell threshold is reached, the system is still metastable. Therefore the counting of avalanches should be interrupted at the point x_* and in the integral (50) we must put the upper limit at $x_s = x_*$, see Fig. 10d. Moreover, in this case, the function $h(x)$ will attain its minimum in the boundary point x_* which slightly modifies the standard saddle point argument (de Bruijn, 2014). Indeed, suppose that at such point $h'(x_*) > 0$. Assume further that $h(x) \rightarrow \infty$, as $x \rightarrow -\infty$ and that the integral $\int_{-\infty}^{x_*} e^{-h(x)} dx$ converges. Then, in the limit $N \rightarrow \infty$ we can write $\int_{-\infty}^{x_*} e^{-Nh(x)} dx \rightarrow e^{Nh(x_*)}/(Nh'(x_*))$. This allow us to re-write the integral (50) in the form

$$p_a(\Delta) \approx \frac{\Delta^{-3/2}}{\sqrt{2\pi}} \frac{e^{-\Delta h(x_*)}}{\Delta h'(x_*)} \phi(x_*) \approx \frac{\phi(x_*)}{h'(x_*)} \frac{\Delta^{-5/2}}{\sqrt{2\pi}} e^{-\Delta(h(x_*))}. \tag{59}$$

The desired scaling relation is then

$$p_a(\Delta) \sim \Delta^{-\alpha} e^{-\Delta(1-h(x_*))}, \tag{60}$$

with $\alpha = 5/2$. Note that the power law scaling is compromised at the large avalanche sizes by an exponential cut off.

All these analytical results, including the exact values of the exponents, fully support our numerical computations presented in Figs. 8 and 9. We have then analytically shown the existence of two scaling exponents characterizing the behavior of our augmented fiber bundle model. While the classical exponent 5/2 is recovered in the brittle regime, the transition from brittle to the ductile regime is characterized by the new exponent 9/4. Such crossover criticality must be tuned as in the case of classical thermodynamical critical point. Instead, the super-criticality observed in the brittle regime is *robust* and can be associated with the presence of a *spinodal* point.

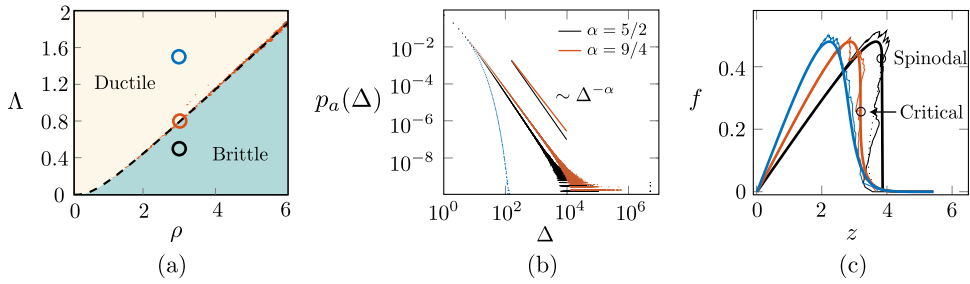


Fig. 11. (a) Brittle-to-ductile transition (critical) line in the (ρ, A) phase diagram. The colored circles in the phase diagram indicate the set of parameters used in (b) and (c). (b) The cumulative avalanche distribution for the system with the corresponding parameters with $N = 10^7$. (c) The superposition of the average force–elongation curve with a realization of system of size $N = 100$.

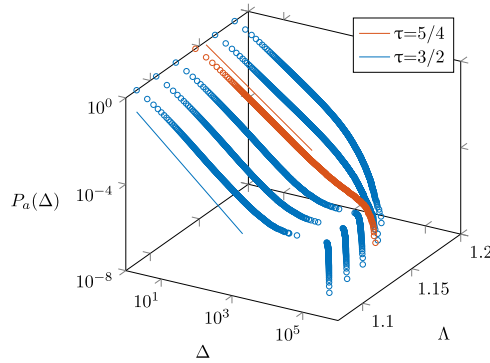


Fig. 12. Cumulative avalanche distribution showing the crossover from ductile to brittle regimes at varying A and fixed disorder (under MS dynamic strategy).

In Fig. 11 we show for the case of MS dynamics and Weibull distribution of thresholds the phase diagram in the rigidity–disorder parameter space exhibiting all three scaling regimes. The crossover region (red) was constructed by applying numerically the Kolmogorov–Smirnov criterion to the power law exponent which was found using the maximum likelihood method (Clauset et al., 2009; Newman, 2005). More specifically, the analysis of the power-law was performed in two steps. First, the parameter α was estimated using the maximum likelihood method. Second, we performed a goodness-of-fit test (using the Kolmogorov method) comparing the obtained avalanche statistics with the power law ansatz found in the previous step. This comparison produced a so called p -value and we assumed that if $p > 0.1$, the power law hypothesis is a plausible representation of the data. Finally, the thick black line in Fig. 11(a), tracing the crossover region, is obtained by solving the two equations $g(x_0; \rho, A) = 1$ and $g'(x_0; \rho, A) = 0$, which is precisely Eq. (23) for the one-parameter Weibull distribution.

In Fig. 12 we use the cumulative distribution of avalanches $P_a(x) = \int^x p_a(s) ds \sim x^{-\tau}$, with $\tau = \alpha - 1$, to illustrate the crossover from the exponent $\tau = 5/2 - 1 = 3/2$ associated with the spinodal criticality to the exponent $\tau = 9/4 - 1 = 5/4$ characterizing the critical point.

6. Finite size scaling

So far, we have been mostly interested in the behavior of the system in the thermodynamic/continuum limit. However, in many applications of fracture mechanics there is a need to understand the effects of finite system size. For instance, in cell cohesion/decohesion phenomena, the area density of proteins responsible for the binding/unbinding is often of the order of a few hundred per μm^2 (Bell, 1978; Erdmann and Schwarz, 2007; Schwarz and Safran, 2013; Erdmann and Schwarz, 2004). In such situations it is of interest to study the effect on the statistics of avalanches of the number of elements N . When N is finite, analytical approach fails and we have to resort to numerical simulations.

Yet, near the critical point some finite N information can be obtained. To show this, suppose first that the dimensionless stiffness of the external spring λ_f , representing the elasticity of the effective environment, is size independent. In this case, the size dependence of the critical distribution of avalanches under MS dynamic protocol is illustrated in Fig. 13. Clearly, the large event cut-off in this case is size dependent.

To understand the structure of the cut-off functions, which are also expected to be universal near the critical point, we write the cumulative probability distribution in the form

$$P_a(\Delta) = \Delta^{-\tau} \mathcal{G}(\Delta/\Delta_c). \tag{61}$$

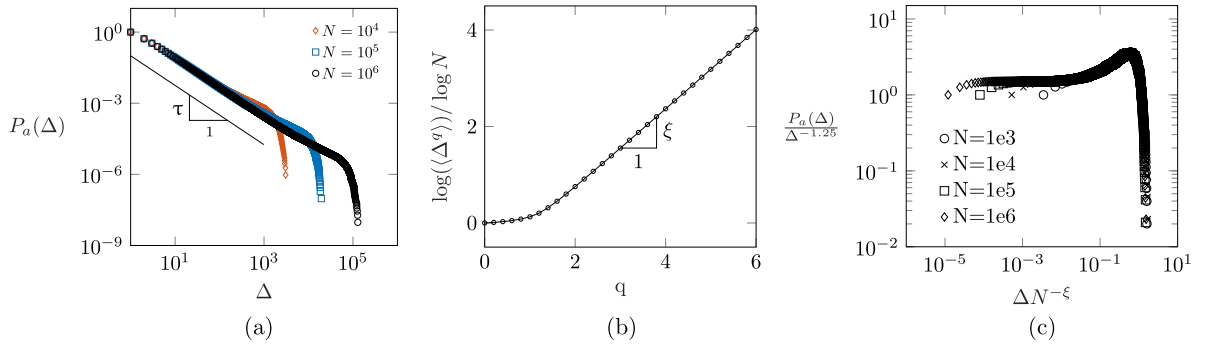


Fig. 13. (a) Avalanche cumulative distribution for the system in the critical state for several system sizes. (b) Plot of the moment spectrum for the distribution of avalanches Δ . The linear part has a slope $\xi \approx 0.8$. (c) Data collapse analysis for the avalanche distribution. The values for the critical exponents are $\tau = 1.25$ and $\xi = 0.8$.

As the system size increases, the cutoff parameter Δ_c is expected to diverge as N^ξ with exponents $\{\tau, \xi\}$ both characterizing the universality class of the model.

To test such finite size scaling (FSS) hypothesis and to find the critical exponent ξ , we performed numerical simulations starting with the values of parameters (ρ, Λ) on the critical line of the averaged system. We conducted simulations at several values of N , adjusting the values of (ρ, Λ) till we covered the whole range of system sizes of interest. The analytically predicted value of the cumulative exponent $\tau = 5/4$ was confirmed. The computation of the exponent ξ was performed through the standard method of moments of $\mathbb{P}(\Delta)$ which reduces to the checking of the hypothesis that $\langle \Delta^q \rangle \sim N^{\xi(q+1-\tau)}$ (Chessa et al., 1999).

In Fig. 13(b), we demonstrate that the conjectured FSS behavior emerges starting from $q = 1.8$. This result is confirmed by the data collapse for the re-scaled distribution $P_a(\Delta, N)\Delta^\tau$ vs. $\Delta N^{-\xi}$, where we use the exponents $\tau = 5/4$ and $\xi = 0.8$ obtained from the moment analysis, see Fig. 13(c).

Suppose now that the dimensionless stiffness of the external spring λ_f varies with the system size N . Since $\lambda_f = \kappa_f/\kappa N$, this means that we no longer assume that $\kappa_f \sim N$. Formally, the dimensional stiffness κ_f characterizes a single linear spring connected in series to the parallel bundle of nonlinear breakable springs. However, the mean-field nature of the model hides the actual spatial structure of the system where each breakable element may interact indirectly with any other breakable element as it is the case, for instance, in a 2D RFM. Such interactions can be represented effectively in our model by various assumptions about the N dependence of κ_f .

Assume that $\kappa_f \sim N^\beta$, where the exponent $0 \leq \beta \leq 1$ can be seen as the (potentially fractional) dimensionality of the load transmitting network. The simplest assumption would be that there is indeed an external N -independent elastic environment which would mean that $\beta = 0$. Then $\Lambda = \lambda_f(\lambda + 1)/\lambda \sim 1/N$. Another limiting case, which we have studied in detail above, is when $\kappa_f \sim N$ which would mean that such external elasticity is extensive and $\beta = 1$ so that Λ is size independent. One can also argue that in the simple tension test for a 3D body whose volume scales as $L^3 \sim N$, the load is applied on a surface with dimension $L^2 \sim N^{2/3}$. Then, if κ_f is to represent the elasticity of the coupling between the load device and the body, we should have $\kappa_f \sim N^{2/3}$ which means that $\beta = 2/3$ and $\Lambda \sim N^{-2/3}$.

Consider, specifically, the case when κ_f is fixed and $\beta = 0$. Then increasing Λ at a fixed λ would mean decreasing N and therefore increased ductility can be viewed as a small size effect. We assume that our analytical results targeting the thermodynamic limit $N \rightarrow \infty$ can be still used to capture such size effect if we simply set $\lambda_f \sim 1/N$. To show that the N dependence of Λ represents the main effect we first write $\Lambda = \tilde{\Lambda}/N$, and assume that the effective rigidity of the system is now characterized by the *size independent* parameter $\tilde{\Lambda}$. We can then construct the curves $z(x)$ at different N but with fixed $\tilde{\Lambda}$.

In Fig. 14(a, b) we compare the corresponding numerically obtained response curves for particular realizations of disorder with the analytical results in the thermodynamic limit where we used the parametric dependence on N through Λ . As we see, the agreement is already good for $N \sim 100$, and particular $\tilde{\Lambda}$. In this figure we see how the BTD transition is captured as a size effect. In contrast to what we have seen in the thermodynamic limit, now the BTD transition is not abrupt but is represented by an extended *critical region*.

This region is clearly visible in Fig. 15 where we show the phase diagram which is based on direct numerical simulations of the system at a given (ρ, N) . The diagram shows three domains with a structurally different distribution of avalanches. In the perforated (red) domain, we observed the power law distribution of avalanches with exponent $\alpha = 9/4$ indicating criticality. In the brittle (blue) domain, we could identify the super-critical avalanche distribution with exponent $\alpha = 5/2$. This is our regime of robust spinodal criticality. Finally, in the ductile (yellow) domain, the power law scaling is absent. To assess the quality of the power laws we estimated the scaling exponent using maximum likelihood method, and then tested the power law hypothesis using the Kolmogorov–Smirnov criterion (Clauset et al., 2009; Newman, 2005; Baró and Vives, 2012).

According to the phase diagram presented in Fig. 15, large systems will be brittle with pseudo-critical avalanche distribution dominated by a large catastrophic (SNAP) events. This observation suggests that the ductile (quasi-brittle) regime can only exist as a finite size effect disappearing in the thermodynamic limit, see also (Dussi et al., 2020). As the size of the system decreases, the

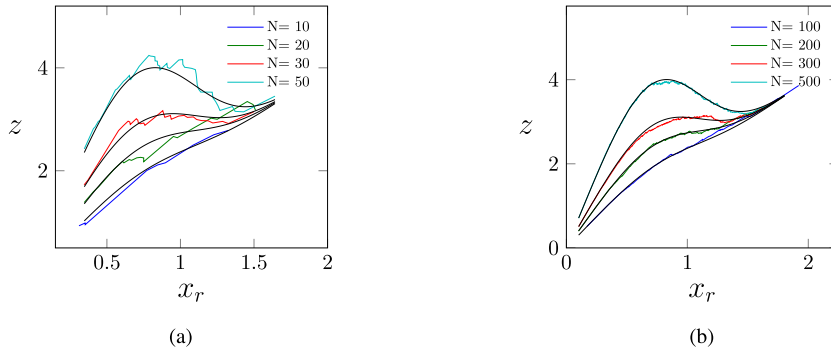


Fig. 14. The effect of the system size on the overall response of the system for two values of the fixed rigidity measure: $\tilde{\lambda} = 20$ (a) and $\tilde{\lambda} = 200$ (b). The colored curves are single realizations of disorder; in black we show the averaged curves obtained by solving (16).

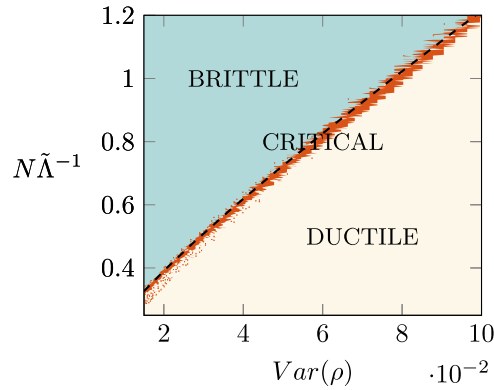


Fig. 15. The effect of the system size N in the overall response of the bundle for $\tilde{\lambda} = 2 \times 10^4$ and $\lambda = 1$ as function of the variance of the disorder $\text{Var}(\rho) = \Gamma(1 + 2/\rho) - [\Gamma(1 + 1/\rho)]^2$ (Weibull distribution), see also a related empirical diagram in (Richard et al., 2021). The diffuse red region shows the uncertainty of interpreting statistics of avalanches as a power law.

spanning events progressively disappear, giving rise to robust scaling with correlation length reaching the system size. Fluctuations (avalanches) take the form of a *crackling* noise with a cut-off. The real (percolation type) criticality in such setting can be observed only in a single point corresponding to an infinite (brittle) system with an infinitely broad disorder. As the system size is decreased further the correlation length becomes microscopic and the system enters the ductile (POP) regime with largely Gaussian statistics of avalanches. Smaller systems naturally place limits on the size of the bursts, which eliminates large events and extends the range of the post cut-off ductile response.

Similar size effect was identified in numerical simulations of the 2D RFM (Shekhawat et al., 2013), where our ductile regime was interpreted as damage percolation, and the analog of our brittle regime was associated with crack nucleation; in view of the implicit identification of the analog of our rigidity measure Λ with $1/N$ the scaling in the crossover region at a given disorder was interpreted as a finite size criticality. The same type of size dependence of the avalanche distribution was also observed in the study of self-organized criticality in a cellular automaton model of earthquakes (Olami et al., 1992); other related results can be found in (Herrmann and Roux, 2014; Toussaint and Hansen, 2006; Delaplace et al., 1996; de Arcangelis and Herrmann, 1989). In all considered cases, three types of breakdown processes were identified: localization, diffuse localization, and percolation-like regime. The numerical study of transitions between different regimes also suggested the existence of an extended region of intermediate system sizes where the critical scaling is robust. This comparison shows that our analytically transparent mean field model captures adequately all the main qualitative features of the more comprehensive 2D lattice models.

7. Conclusions

We used a prototypical model of fracture in disordered solids to quantify the role of the system's rigidity (global connectivity) as a control parameter for the transition from brittle to ductile failure. The ductile response is usually associated with the stable development of small avalanches (micro-bursts), representing debonding events at the microscopic level. Instead, the brittle response is associated with large system-size events representing macro-crack-type system-size instabilities. In our model, the two types of fracture are distinguished by their statistical distribution of bond-breaking avalanches.

More specifically, we showed that the avalanche statistics associated with brittle regimes could be interpreted as resulting from spinodal instability. These regimes, however, cannot be called critical because of the presence of system size events signifying global failure. The complete criticality of crackling type (Sethna et al., 2001), is observed exactly at the brittle-to-ductile transition, which can be identified (at infinite disorder if $\beta = 0$) with the classical thermodynamic critical point. In the fully developed ductile regime, intermittency is lost and the distribution of fracture avalanches can be interpreted as a succession of uncorrelated events.

One of our main conclusions is that the brittle-to-ductile transition can be associated with the crossover from spinodal to classical criticality, generating, in finite size systems, a scaling region with nonuniversal exponents. Such behavior is generic for a broad class of systems, encompassing fracture, plasticity, structural phase transitions, and even fluid turbulence. Our analysis reveals that in the transition region on the phase diagram, the system following the marginal stability (MS) dynamics exhibits an avalanche size distribution exponent different from the one associated with the robust spinodal criticality, characterizing brittle regimes. In the setting of global minimization (GM) dynamics, we observe a universal power-law distribution of avalanches only in the transition from brittle to the ductile regime with the same exponent as encountered under MS dynamics. One can then argue that the robust criticality, as in the case of earthquakes and collapse of compressed porous materials, should result from some feedback mechanisms ensuring self-tuning of the system towards the border separating brittle and ductile behaviors. Our study indicates that in addition to the strength of disorder, an appropriately chosen global measure of rigidity can also serve as an instrument of such tuning.

The results obtained in our fully analytical study of the mean-field model of fracture in a disordered system can be used only for qualitative guidance in developing acoustic-emission-based precursors for global failure. Quantitative predictions should be, of course, based on the analysis of the comprehensive numerical models of realistic systems. And yet, we emphasize that the present prototypical model has already captured the principal features of such systems, including the presence of different scaling regimes in the space of disorder-rigidity parameters. Therefore, the obtained results can already serve as a basic guide in the design of new materials. In particular, our study unveils the possibility of using the statistical signature of stochastic fluctuations for non-destructive acoustic monitoring of the remaining life of fracturing samples. By omitting some details, available only through the study of purely numerical models, this simple analytical model reveals the quantitative importance of collective effects and long-range correlations in fracture development. In this sense, it provides new fundamental insights into the mechanism of failure in disordered solids.

CRediT authorship contribution statement

Hudson Borja da Rocha: Conceptualization, Investigation, Writing. **Lev Truskinovsky:** Conceptualization, Investigation, Writing.

Declaration of competing interest

The authors declare that they have no known competing financial interests or personal relationships that could have appeared to influence the work reported in this paper.

Acknowledgments

The authors are grateful to R. Garcia-Garcia and M. Mungan for helpful discussions. H. B. R. was supported by a Ph.D. fellowship from Ecole Polytechnique; L. T. was supported by Grant No. ANR-10-IDEX-0001-02 PSL, France.

References

- Alava, M.J., Nukala, P.K.V.V., Zapperi, S., 2006. Statistical models of fracture. *Adv. Phys.* 55 (3–4), 349–476. <http://dx.doi.org/10.1080/00018730300741518>.
- de Arcangelis, L., Herrmann, H.J., 1989. Scaling and multiscaling laws in random fuse networks. *Phys. Rev. B* 39, 2678–2684. <http://dx.doi.org/10.1103/PhysRevB.39.2678>.
- de Arcangelis, L., Redner, S., Herrmann, H.J., 1985. A random fuse model for breaking processes. *J. Phys. Lett.* 46 (13), 585–590. <http://dx.doi.org/10.1051/jphyslet:019850046013058500>.
- Balog, I., Tissier, M., Tarjus, G., 2014. Same universality class for the critical behavior in and out of equilibrium in a quenched random field. *Phys. Rev. B* 89, 104201. <http://dx.doi.org/10.1103/PhysRevB.89.104201>.
- Baró, Jordi, Dahmen, Karin A., Davidsen, Jörn, Planes, Antoni, Castillo, Pedro O., Nataf, Guillaume F., Salje, Ekhard K. H., Vives, Eduard, 2018. Experimental evidence of accelerated seismic release without critical failure in acoustic emissions of compressed nanoporous materials. *Phys. Rev. Lett.* 120, 245501. <http://dx.doi.org/10.1103/PhysRevLett.120.245501>.
- Baró, J., Vives, E., 2012. Analysis of power-law exponents by maximum-likelihood maps. *Phys. Rev. E* 85, 066121. <http://dx.doi.org/10.1103/PhysRevE.85.066121>.
- Bažant, Z.P., 2019. Design of quasibrittle materials and structures to optimize strength and scaling at probability tail: an apercu. *Proc. R. Soc. Lond. Ser. A Math. Phys. Eng. Sci.* 475 (2224), 20180617. <http://dx.doi.org/10.1098/rspa.2018.0617>.
- Bazant, Z.P., Le, J.-L., 2017. *Probabilistic Mechanics of Quasibrittle Structures: Strength, Lifetime, and Size Effect*. Cambridge University Press.
- Bell, G., 1978. Models for the specific adhesion of cells to cells. *Sci.* 200 (4342), 618–627. <http://dx.doi.org/10.1126/science.347575>.
- Berthier, Estelle, Démery, Vincent, Ponson, Laurent, 2017. Damage spreading in quasi-brittle disordered solids: I. localization and failure. *Journal of the Mechanics and Physics of Solids* (ISSN: 0022-5096) 102, 101–124. <http://dx.doi.org/10.1016/j.jmps.2016.08.013>.
- Berthier, E., Kollmer, J.E., Henkes, S.E., Liu, K., Schwarz, J.M., Daniels, K.E., 2019. Rigidity percolation control of the brittle–ductile transition in disordered networks. *Phys. Rev. Mater.* 3, 075602. <http://dx.doi.org/10.1103/PhysRevMaterials.3.075602>.
- Berthier, Estelle, Mayya, Ashwji, Ponson, Laurent, 2021. Damage spreading in quasi-brittle disordered solids: II. What the statistics of precursors teach us about compressive failure.
- Biswas, S., Ray, P., Chakrabarti, B.K., 2015. *Statistical Physics of Fracture, Breakdown, and Earthquake: Effects of Disorder and Heterogeneity*. John Wiley & Sons.

- Bonamy, D., Bouchaud, E., 2011. Failure of heterogeneous materials: A dynamic phase transition? *Phys. Rep.* 498 (1), 1–44. <http://dx.doi.org/10.1016/j.physrep.2010.07.006>.
- Bouchbinder, E., Goldman, T., Fineberg, J., 2014. The dynamics of rapid fracture: instabilities, nonlinearities and length scales. *Rep. Progr. Phys.* 77 (4), 046501. <http://dx.doi.org/10.1088/0034-4885/77/4/046501>.
- Bourdin, B., Francfort, G.A., Marigo, J.-J., 2008. The variational approach to fracture. *J. Elasticity* 91 (1–3), 5–148.
- de Bruijn, N., 2014. *Asymptotic Methods in Analysis*, Dover Books on Mathematics. Dover Publications.
- Caruel, M., Truskinovsky, L., 2017. Bi-stability resistant to fluctuations. *J. Mech. Phys. Solids* 109, 117–141. <http://dx.doi.org/10.1016/j.jmps.2017.08.007>.
- Chessa, A., Vespignani, A., Zapperi, S., 1999. Critical exponents in stochastic sandpile models. *Comput. Phys. Comm.* 121, 299–302.
- Christensen, R., Li, Z., Gao, H., 2018. An evaluation of the failure modes transition and the christensen ductile/brittle failure theory using molecular dynamics. *Proc. R. Soc. Lond. Ser. A Math. Phys. Eng. Sci.* 474 (2219), 20180361. <http://dx.doi.org/10.1098/rspa.2018.0361>.
- Clauset, A., Shalizi, C.R., Newman, M.E.J., 2009. Power-law distributions in empirical data. *SIAM Rev.* 51 (4), 661–703. <http://dx.doi.org/10.1137/070710111>.
- Crapo, Henry, 1979. *Structural rigidity. Structural topology*, 1979, núm. 1.
- Curtin, W., 1998. Stochastic damage evolution and failure in fiber-reinforced composites. *Adv. Appl. Mech.* 36, 163–253.
- David, R., Corrado, R., Edan, L., 2021. Finite-size study of the athermal quasistatic yielding transition in structural glasses. [arXiv:2104.02441](https://arxiv.org/abs/2104.02441).
- Delaplace, A., Pijaudier-Cabot, G., Roux, S., 1996. Progressive damage in discrete models and consequences on continuum modelling. *J. Mech. Phys. Solids* 44 (1), 99–136. [http://dx.doi.org/10.1016/0022-5096\(95\)00062-3](http://dx.doi.org/10.1016/0022-5096(95)00062-3).
- Delaplace, A., Roux, S., Jaudier Cabot, G.P., 1999. Damage cascade in a softening interface. *Int. J. Solids Struct.* 36 (10), 1403–1426. [http://dx.doi.org/10.1016/S0020-7683\(98\)00054-7](http://dx.doi.org/10.1016/S0020-7683(98)00054-7).
- Deng, B., Shi, Y., 2018. On measuring the fracture energy of model metallic glasses. *J. Appl. Phys.* 124 (3), 035101. <http://dx.doi.org/10.1063/1.5037352>.
- Driscoll, M.M., G.-g. Chen, B., Beuman, T.H., Ulrich, S., Nagel, S.R., Vitelli, V., 2016. The role of rigidity in controlling material failure. *Proc. Natl. Acad. Sci.* 113 (39), 10813–10817. <http://dx.doi.org/10.1073/pnas.1501169113>.
- Dussi, S., Tauber, J., van der Gucht, J., 2020. Athermal fracture of elastic networks: How rigidity challenges the unavoidable size-induced brittleness. *Phys. Rev. Lett.* 124, 018002. <http://dx.doi.org/10.1103/PhysRevLett.124.018002>.
- Efendiev, Y.R., Truskinovsky, L., 2010. Thermalization of a driven bi-stable fpu chain. *Contin. Mech. Thermodyn.* 22 (6), 679–698.
- Erdmann, T., Schwarz, U.S., 2004. Stability of adhesion clusters under constant force. *Phys. Rev. Lett.* 92, 108102. <http://dx.doi.org/10.1103/PhysRevLett.92.108102>.
- Erdmann, T., Schwarz, U., 2007. Impact of receptor–ligand distance on adhesion cluster stability. *Eur. Phys. J. E* 22, 123–137.
- Feller, W., 1968. *An Introduction To Probability Theory and Its Applications*. Vol. 1, Wiley.
- Fortin, Jerome, Stanchits, Sergei, Dresen, Georg, Gueguen, Yves, 2009. Acoustic emissions monitoring during inelastic deformation of porous sandstone: comparison of three modes of deformation. In: Vinciguerra, Sergio, Bernabé, Yves (Eds.), *Rock Physics and Natural Hazards*. Birkhäuser Basel, ISBN: 978-3-0346-0122-1, pp. 823–841. http://dx.doi.org/10.1007/978-3-0346-0122-1_5.
- Francfort, G., Marigo, J.-J., 1998. Revisiting brittle fracture as an energy minimization problem. *J. Mech. Phys. Solids* 46 (8), 1319–1342. [http://dx.doi.org/10.1016/S0022-5096\(98\)00034-9](http://dx.doi.org/10.1016/S0022-5096(98)00034-9).
- Garcimartín, A., Guarino, A., Bellón, L., Ciliberto, S., 1997. Statistical properties of fracture precursors. *Phys. Rev. Lett.* 79, 3202–3205. <http://dx.doi.org/10.1103/PhysRevLett.79.3202>.
- Girard, L., Amitrano, D., Weiss, J., 2010. Failure as a critical phenomenon in a progressive damage model. *Journal of Statistical Mechanics: Theory and Experiment* 2010 (1), P01013. <http://dx.doi.org/10.1088/1742-5468/2010/01/p01013>.
- Goodrich, C.P., Liu, A.J., Nagel, S.R., 2014. Solids between the mechanical extremes of order and disorder. *Nat. Phys.* 10 (8), 578–581. <http://dx.doi.org/10.1038/nphys3006>.
- Gorgogianni, Anna, Eliáš, Jan, Le, Jia-Liang, 2020. Mechanism-based energy regularization in computational modeling of quasibrittle fracture. *Journal of Applied Mechanics (ISSN: 0021-8936)* 87 (9), 091003. <http://dx.doi.org/10.1115/1.4047207>.
- Greeves, G.N., Greer, A.L., Lakes, R.S., Rouxel, T., 2011. Poisson's ratio and modern materials. *Nature Mater.* 10 (11), 823–837. <http://dx.doi.org/10.1038/nmat3134>.
- Halász, Z., Kun, F., 2010. Slip avalanches in a fiber bundle model. *Europhys. Lett.* 89 (2), 26008.
- Hansen, A., Hemmer, P.C., 1994. Criticality in fracture: the burst distribution. *Trends Stat. Phys.* 1 (213).
- Hansen, A., Hemmer, P., Pradhan, S., 2015. *The Fiber Bundle Model: Modeling Failure in Materials, Statistical Physics of Fracture and Breakdown*. Wiley.
- Hansen, A., Roux, S., 2000. Statistics toolbox for damage and fracture. In: Krajcinovic, D., Van Mier, J. (Eds.), *Damage and Fracture of Disordered Materials*. Springer Vienna, Vienna, pp. 17–101.
- Hemmer, P.C., Hansen, A., 1992. The distribution of simultaneous fiber failures in fiber bundles. *J. Appl. Mech.* 59 (4), 909–914.
- Herrmann, H., Roux, S., 2014. *Statistical Models for the Fracture of Disordered Media, Random Materials and Processes*. Elsevier Science.
- Kim, J.Z., Lu, Z., Strogatz, S.H., Bassett, D.S., 2019. Conformational control of mechanical networks. *Nat. Phys.* 15 (7), 714–720. <http://dx.doi.org/10.1038/s41567-019-0475-y>.
- Kloster, A.H.M., Hemmer, P.C., 1997. Burst avalanches in solvable models of fibrous materials. *Phys. Rev. E* 56 (3), 2615–2625. <http://dx.doi.org/10.1103/PhysRevE.56.2615>.
- Krajcinovic, D., Van Mier, J., 2000. *Damage and Fracture of Disordered Materials*. Springer.
- Liu, J., Zhao, Z., Wang, W., Mays, J.W., Wang, S.-Q., 2019. Brittle–ductile transition in uniaxial compression of polymer glasses. *J. Polym. Sci.* 57 (12), 758–770. <http://dx.doi.org/10.1002/polb.24830>.
- Merkel, M., Baumgarten, K., Tighe, B.P., Manning, M.L., 2019. A minimal-length approach unifies rigidity in underconstrained materials. *Proc. Natl. Acad. Sci.* 116 (14), 6560–6568. <http://dx.doi.org/10.1073/pnas.1815436116>.
- Metzler, R., Redner, S., Oshanin, G., 2014. *First-Passage Phenomena and their Applications*. Vol. 35, World Scientific.
- Mielke, A., Truskinovsky, L., 2012. From discrete visco-elasticity to continuum rate-independent plasticity: Rigorous results. *Arch. Ration. Mech. Anal.* 203 (2), 577–619.
- Moreno, Y., Gómez, J.B., Pacheco, A.F., 2000. Fracture and second-order phase transitions. *Phys. Rev. Lett.* 85, 2865–2868. <http://dx.doi.org/10.1103/PhysRevLett.85.2865>.
- Nechad, H., Helmstetter, A., El Guerjouma, R., Sornette, D., 2005. Andrade and critical time-to-failure laws in fiber–matrix composites: Experiments and model. *J. Mech. Phys. Solids* 53 (5), 1099–1127. <http://dx.doi.org/10.1016/j.jmps.2004.12.001>.
- Newman, M.E., 2005. Power laws pareto distributions and zipf's law. *Contemp. Phys.* 46 (5), 323–351.
- Nikolić, M., Karavelić, E., Ibrahimbegović, A., Mišćević, P., 2018. Lattice element models and their peculiarities. *Arch. Comput. Methods Eng.* 1183, 753–784. <http://dx.doi.org/10.1007/s11831-017-9210-y>.
- Olami, Z., Feder, H.J.S., Christensen, K., 1992. Self-organized criticality in a continuous, nonconservative cellular automaton modeling earthquakes. *Phys. Rev. Lett.* 68, 1244–1247. <http://dx.doi.org/10.1103/PhysRevLett.68.1244>.
- Østergaard, Martin B., Hansen, Søren R., Januchta, Kacper, To, Theany, Rzoska, Sylwester J., Bockowski, Michal, Bauchy, Mathieu, Smedskaer, Morten M., 2019. Revisiting the dependence of Poisson's ratio on liquid fragility and atomic packing density in oxide glasses. *Materials* 12 (15), 2439. <http://dx.doi.org/10.3390/ma12152439>.
- Ostoja-Starzewski, M., 2007. *Microstructural Randomness and Scaling in Mechanics of Materials*. CRC Press.

- Papanikolaou, S., Shanthraj, P., Thibault, J., Woodward, C., Roters, F., 2019. Brittle to quasi-brittle transition and crack initiation precursors in crystals with structural inhomogeneities. *Mater. Theory* 3 (1), 5. <http://dx.doi.org/10.1186/s41313-019-0017-0>.
- Patinet, S., Vandembroucq, D., Hansen, A., Roux, S., 2014. Cracks in random brittle solids. *Eur. Phys. J. Spec. Top.* 223 (1), 2339–2351. <http://dx.doi.org/10.1140/epjst/e2014-02268-9>.
- Petri, A., Paparo, G., Vespignani, A., Alippi, A., Costantini, M., 1994. Experimental evidence for critical dynamics in microfracturing processes. *Phys. Rev. Lett.* 73, 3423–3426. <http://dx.doi.org/10.1103/PhysRevLett.73.3423>.
- Politi, A., Ciliberto, S., Scorretti, R., 2002. Failure time in the fiber-bundle model with thermal noise and disorder. *Phys. Rev. E* 66, 026107. <http://dx.doi.org/10.1103/PhysRevE.66.026107>.
- Pradhan, S., Hansen, A., Chakrabarti, B.K., 2010. Failure processes in elastic fiber bundles. *Rev. Modern Phys.* 82 (1), 499–555. <http://dx.doi.org/10.1103/RevModPhys.82.499>.
- Puglisi, G., Truskinovsky, L., 2005. Thermodynamics of rate-independent plasticity. *J. Mech. Phys. Solids* 53 (3), 655–679. <http://dx.doi.org/10.1016/j.jmps.2004.08.004>.
- Ray, P., 2019. Statistical physics perspective of fracture in brittle and quasi-brittle materials. *Phil. Trans. R. Soc. A* 377 (2136), 20170396. <http://dx.doi.org/10.1098/rsta.2017.0396>.
- Richard, D., Lerner, E., Bouchbinder, E., 2021. Brittle to ductile transitions in glasses: Roles of soft defects and loading geometry. [arXiv:2103.05258](https://arxiv.org/abs/2103.05258).
- Borja da Rocha, H., Truskinovsky, L., 2019. Equilibrium unzipping at finite temperature. *Arch. Appl. Mech.* 89 (3), 535–544. <http://dx.doi.org/10.1007/s00419-018-1485-4>.
- Borja da Rocha, H., Truskinovsky, L., 2020. Rigidity-controlled crossover: From spinodal to critical failure. *Phys. Rev. Lett.* 124, 015501. <http://dx.doi.org/10.1103/PhysRevLett.124.015501>.
- Roux, S., 2000. Thermally activated breakdown in the fiber-bundle model. *Phys. Rev. E* 62, 6164–6169. <http://dx.doi.org/10.1103/PhysRevE.62.6164>.
- Sahimi, M., 1998. Non-linear and non-local transport processes in heterogeneous media: from long-range correlated percolation to fracture and materials breakdown. *Phys. Rep.* 306 (4), 213–395. [http://dx.doi.org/10.1016/S0370-1573\(98\)00024-6](http://dx.doi.org/10.1016/S0370-1573(98)00024-6).
- Schwarz, U.S., Safran, S.A., 2013. Physics of adherent cells. *Rev. Modern Phys.* 85, 1327–1381. <http://dx.doi.org/10.1103/RevModPhys.85.1327>.
- Selezneva, M., Swolfs, Y., Katalagarianakis, A., Ichikawa, T., Hirano, N., Taketa, I., Karaki, T., Verpoest, I., Gorbatiikh, L., 2018. The brittle-to-ductile transition in tensile and impact behavior of hybrid carbon fibre/self-reinforced polypropylene composites. *Composites A* 109, 20–30. <http://dx.doi.org/10.1016/j.compositesa.2018.02.034>.
- Selinger, R.L.B., Wang, Z.-G., Gelbart, W.M., 1991. Effect of temperature and small-scale defects on the strength of solids. *J. Chem. Phys.* 95 (12), 9128–9141. <http://dx.doi.org/10.1063/1.461192>.
- Sethna, J.P., Dahmen, K.A., Myers, C.R., 2001. Crackling noise. *Nature* 410, 242–250. <http://dx.doi.org/10.1038/35065675>.
- Shekhawat, A., Zapperi, S., Sethna, J.P., 2013. From damage percolation to crack nucleation through finite size criticality. *Phys. Rev. Lett.* 110, 185505. <http://dx.doi.org/10.1103/PhysRevLett.110.185505>.
- Sornette, D., 1989. Elasticity and failure of a set of elements loaded in parallel. *J. Phys. A: Math. Gen.* 22 (6), L243.
- Sornette, Didier., 1992. Mean-field solution of a block-spring model of earthquakes. *J. Phys. I France* 2 (11), 2089–2096. <http://dx.doi.org/10.1051/jp1:1992269>.
- Sornette, Didier., 2002. Predictability of catastrophic events: material rupture, earthquakes, turbulence, financial crashes, and human birth. *Proceedings of the National Academy of Sciences (ISSN: 0027-8424)* 99 (suppl 1), 2522–2529. <http://dx.doi.org/10.1073/pnas.022581999>.
- Sornette, D., 2006. *Critical Phenomena in Natural Sciences: Chaos, Fractals, Selforganization and Disorder: Concepts and Tools*. Springer Science & Business Media.
- Tordesillas, Antoinette, Kahagalage, Sanath, Ras, Charl, Nitka, Michał, Tejchman, Jacek, 2020. Coupled evolution of preferential paths for force and damage in the pre-failure regime in disordered and heterogeneous, quasi-brittle granular materials. *Frontiers in Materials (ISSN: 2296-8016)* 7, 79. <http://dx.doi.org/10.3389/fmats.2020.00079>.
- Toussaint, R., Hansen, A., 2006. Mean-field theory of localization in a fuse model. *Phys. Rev. E* 73, 046103. <http://dx.doi.org/10.1103/PhysRevE.73.046103>.
- Vermeulen, M.F.J., Bose, A., Storm, C., Ellenbroek, W.G., 2017. Geometry and the onset of rigidity in a disordered network. *Phys. Rev. E* 96, 053003. <http://dx.doi.org/10.1103/PhysRevE.96.053003>.
- Vu, Chi-Cong, Amitrano, David, Plé, Olivier, Weiss, Jérôme, 2019. Compressive failure as a critical transition: experimental evidence and mapping onto the universality class of depinning. *Phys. Rev. Lett.* 122 (1), 015502. <http://dx.doi.org/10.1103/PhysRevLett.122.015502>.
- Wang, Z.-G., Landman, U., Selinger, R.L.B., Gelbart, W.M., 1991. Molecular-dynamics study of elasticity and failure of ideal solids. *Phys. Rev. B* 44, 378–381. <http://dx.doi.org/10.1103/PhysRevB.44.378>.
- Weiss, Jérôme, Girard, Lucas, Gimbert, Florent, Amitrano, David, Vandembroucq, Damien, 2014. (Finite) statistical size effects on compressive strength. *Proceedings of the National Academy of Sciences (ISSN: 0027-8424)* 111 (17), 6231–6236. <http://dx.doi.org/10.1073/pnas.1403500111>.
- Xia, Z., Curtin, W., Peters, P., 2001. Multiscale modeling of failure in metal matrix composites. *Acta Mater.* 49 (2), 273–287. [http://dx.doi.org/10.1016/S1359-4464\(00\)00317-7](http://dx.doi.org/10.1016/S1359-4464(00)00317-7).
- Zapperi, S., Ray, P., Stanley, H.E., Vespignani, A., 1997. First-order transition in the breakdown of disordered media. *Phys. Rev. Lett.* 78, 1408–1411. <http://dx.doi.org/10.1103/PhysRevLett.78.1408>.
- Zhang, L., Rocklin, D.Z., Sander, L.M., Mao, X., 2017. Fiber networks below the isostatic point: Fracture without stress concentration. *Phys. Rev. Mater.* 1, 052602. <http://dx.doi.org/10.1103/PhysRevMaterials.1.052602>.